Research Article

The incorporation of chlorine and cosmogenic ^{36}Cl into speleothem carbonate

Vanessa E. Johnston[a,b,†] ![ORCID], Silvia Frisia[c,d], Andrea Borsato[b,c], Jon D. Woodhead[e] and Frank McDermott[a]

[a]UCD School of Earth Sciences, University College Dublin, Belfield, Dublin 4, Ireland; [b]Museo delle Scienze, Corso del Lavoro e della Scienza 3, 38122 Trento, Italy; [c]School of Environmental and Life Sciences, University of Newcastle, Callaghan, 2308 New South Wales, Australia; [d]School of Biological, Earth and Environmental Sciences, University of New South Wales, Sydney, 2052 New South Wales, Australia and [e]School of Geography, Earth and Atmospheric Sciences, The University of Melbourne, 3010 Victoria, Australia

Abstract

Cave carbonate mineral deposits (speleothems) contain trace elements that are intensively investigated for their significance as palaeoclimate and environmental proxies. However, chlorine, which is abundant in marine and meteoric waters, has been overlooked as a potential palaeo-proxy, while cosmogenic ^{36}Cl could, in principle, provide a solar irradiance proxy. Here, total Cl concentrations analysed from various speleothems were low (3–14 mg/kg), with variations linked to crystal fabrics. High-resolution synchrotron radiation micro X-ray fluorescence (μ-XRF) trace element mapping showed Cl often associated with Na, Si, and Al. We propose that speleothems incorporate Cl in two fractions: (1) water soluble (e.g., fluid inclusions) and (2) water insoluble and strongly bound (e.g., associated with detrital particulates). However, disparities indicated that alternate unidentified mechanisms for Cl incorporation were present, raising important questions regarding incorporation of many trace elements into speleothems. Our first measurements of ^{36}Cl/Cl ratios in speleothems required large samples due to low Cl concentrations, limiting the potential of ^{36}Cl as a solar irradiance proxy. Critically, our findings highlight a knowledge gap into how Cl and other trace elements are incorporated into speleothems, how the incorporation mechanisms and final elemental concentrations are related to speleothem fabrics, and the significance this may have for how trace elements in speleothems are interpreted as palaeoclimate proxies.

Keywords: Speleothem chlorine concentration, Speleothem fabrics, Synchrotron radiation micro X-ray fluorescence trace element maps, Instrumental neutron activation analysis, Chlorine-36, Cosmogenic isotopes

(Received 13 February 2023; accepted 16 October 2023)

INTRODUCTION

Cosmogenic isotopes (e.g., ^{14}C, ^{10}Be, and ^{36}Cl) are important proxies for solar (e.g., Bard et al., 1997) and geomagnetic activity (e.g., Christl et al., 2004; Muscheler et al., 2005). The production of cosmogenic isotopes depends on the flux of galactic cosmic rays (GCR) into the Earth's atmosphere, which varies as a function of the strength of the geomagnetic field (on multimillennial timescales) and solar activity (on decadal to millennial timescales) (Lal and Peters, 1967). A strong solar "wind," associated with high solar activity, deflects GCR away from the Earth, resulting in lower production rates of cosmogenic isotopes. This inverse relationship between solar activity and the cosmogenic nuclide production rate is the basis for their use as proxies for solar irradiance reconstruction (Usoskin et al., 2009).

Caves offer archives in both sediment deposits and speleothems that could potentially preserve records of cosmogenic isotope ratios due to bedrock shielding from bombardment of GCR and surface erosional processes. Clastic sediments in caves have been investigated for cosmogenic isotope dating (e.g., Stock et al., 2005); however, the ages differed by an order of magnitude when compared with those of speleothems in the same layer. Therefore, despite its potential to provide a geomorphic record of cave river system evolution (White, 2007), dating of cave sediments through cosmogenic isotopes is still rare in the literature. On the other hand, speleothem dating by the U-series method is robust and well established, making these cave mineral formations an excellent repository of palaeoclimate proxies, such as C and O isotope ratios and trace elements (e.g., McDermott, 2004; Fairchild and Treble, 2009). Robust chronologies of speleothems have been already obtained by using radiocarbon (^{14}C)—perhaps the most well-known cosmogenic isotope (e.g., Lechleitner et al., 2016). Given the relationship between ^{14}C production and solar activity, geological archives such as speleothems could allow the assessment of the long-term effects of solar irradiance forcing on climate (e.g., Scholz et al., 2012).

Radiocarbon has indeed already been recognised as a crucial proxy for disentangling complex relationships between solar activity, vegetation processes, and water–rock interactions in speleothems (e.g., Beck et al., 2001; Jackson et al., 2008; Faraji et al., 2023). However, ^{14}C use as a palaeo–solar irradiance proxy in speleothems is hampered by its relatively short half-life and

complexities relating to uptake and recycling in the biosphere, as well as its sensitivity to variable rock dissolution effects in limestone karst settings. For these reasons, longer-lived cosmogenic nuclides, such as ^{10}Be and ^{36}Cl, that are less affected by biological processes, could offer the potential for reconstructing pre-^{14}C (ca. pre–50,000 years BP), long and reliable, solar and geomagnetic records (Plummer et al., 1997) from speleothems.

In this pilot study, we have chosen to focus on ^{36}Cl due to the existing research about ^{36}Cl in cave waters, which has shown that ^{36}Cl/Cl ratios are faithfully transmitted from rainfall into cave drip water (Johnston and McDermott, 2009; Münsterer et al., 2012; Turin et al., 2022). However, ^{36}Cl has yet to be explored in speleothems, in part because little is known about how Cl is incorporated into speleothem carbonate. We aimed at understanding whether the ^{36}Cl/Cl ratio could be measured in speleothems to subsequently assess the potential of speleothems to provide well-dated, contemporaneous solar irradiance and palaeoclimate proxy records. Because this was a pioneer study, we analysed the Cl concentration of a variety of available speleothem samples to see how Cl concentrations may differ between different speleothem fabrics and across a wide geographic area. In addition, synchrotron radiation micro X-ray fluorescence (μ-XRF) Cl distribution maps that were obtained within a more general framework of understanding how trace elements are incorporated into speleothems were used here to provide insight on where Cl is preferentially concentrated relative to fabrics. We discuss how Cl can be extracted from speleothems for cosmogenic isotope ratio measurements and, finally, we present the first measurements of their ^{36}Cl/Cl ratios. Our observations suggest that Cl is mostly incorporated extra-lattice, and its concentration depends on fabrics. We also found that, with current methodologies, the use of ^{36}Cl in speleothems is hampered by the large amount of sample required, which would result in an insufficient temporal resolution as a solar irradiance proxy.

MATERIALS AND METHODS

The samples used for this study were portions from various specimens, some of which had been previously used in palaeoenvironmental and petrographic/geochemical research (Fig. 1, Table 1). The analytical techniques used in this study were: (1) optical microscopy observations to determine speleothem fabrics; (2) wet chemical leaching methods to extract and measure Cl concentrations; (3) instrumental neutron activation analysis (INAA) to measure total Cl concentrations; (4) synchrotron radiation–based high-resolution μ-XRF trace element mapping to visualise the distribution (but not concentration) of trace elements, including Cl (e.g., Frisia et al., 2012); and (5) accelerator mass spectrometry (AMS) to measure the ^{36}Cl/Cl ratios in speleothems. Because this was a proof-of-concept study, not all the analytical techniques could be applied on every sample due to the limited amount of material, the analytical costs, and the resources available. Namely, smaller samples used for Cl concentration determination and Cl distribution were taken as off-cuts from some speleothems used in the framework of other studies, while the ^{36}Cl/Cl ratios were measured on large speleothems that were not being utilised in other studies due to the destructive nature of the analytical methods (Table 1).

Optical microscopy observations

Speleothem fabrics were observed, when feasible, for 30-μm-thick thin sections, using a Zeiss Axioskop petrographic microscope at the Museo delle Scienze (MUSE, Italy), in both plane-polarized and cross-polarized light modes. Fabrics were classified according to conceptual criteria reported in Frisia (2015) and Frisia et al. (2022). For samples for which not enough material was available to obtain thin sections, fabrics were determined from high-resolution scans of polished specimens (Table 2).

Cl concentrations by leaching

Small samples were broken into chips using a jaw crusher, and approximately 10 g of this material was crushed by hand in a mortar and pestle. A simple, yet effective method of leaching the carbonate powder in deionised water, utilising the hydrophilic behaviour of Cl, obtained the soluble fraction of Cl in the sample, hereafter "water-soluble Cl⁻." An aliquot of the supernatant was removed for analysis of anions by ion chromatography at the University College Dublin, Ireland (Dionex ICS-1000, with AS9-HC column and IonPac AG9-HC guard column, standardised with Sigma-Aldrich multi-element ion chromatography standard solution I) to gain the Cl⁻ concentration in the water, which was then used to calculate the amount of Cl extracted from the sample. Of note, previous experiments to digest speleothem samples in both nitric and phosphoric acids in sealed containers did not improve the Cl yield and introduced a potential source of contamination. Additionally, the same ion chromatography system (Dionex ICS-1000) was used to analyse a small selection of drip waters from the studied caves.

Cl concentrations by INAA

Samples (ca. 1–6 g; Table 2) were crushed by hand in a mortar and pestle. Total Cl concentrations were determined by INAA on these powders at the Becquerel Laboratories Inc., Canada. The results are accredited by ISO 17025 no. 422.

Synchrotron radiation μ-XRF trace element mapping

Three speleothems retrieved from caves in the Nullarbor, South Australia, and one from Moline Cave, NE Italy (Table 1), were investigated by synchrotron radiation–based μ-XRF. The Nullarbor samples were previously studied to unravel the significance of P and its incorporation in speleothem calcite (Frisia et al., 2012). All also yielded Cl distribution data, which are presented here. Speleothem samples for μ-XRF trace element mapping were prepared by double polishing 1-mm-thick wafers, which were subsequently ultrasonically cleaned in deionised water to remove any surface Cl contamination and then handled with sterile gloves to prevent interaction with the skin. Free-standing wafers were inserted in a sample chamber operating at a pressure of 10^{-5} mbar at the ID21 beamline of the European Synchrotron Radiation Facility (ESRF). The excitation energy of the beam was set to 4.5 KeV for the measurement of elements with atomic number lower than Ca, and the analytical spot size was 1 μm diameter. Details of the experimental method can be found in Frisia et al. (2005, 2012).

^{36}Cl/Cl ratios by AMS

^{36}Cl/Cl ratio measurements on carbonates are typically carried out with the aim of determining exposure ages, utilising in situ–produced ^{36}Cl (i.e., ^{36}Cl produced within the carbonate rock itself via GCR bombardment of ^{40}Ca); hence, the ^{36}Cl is held within the
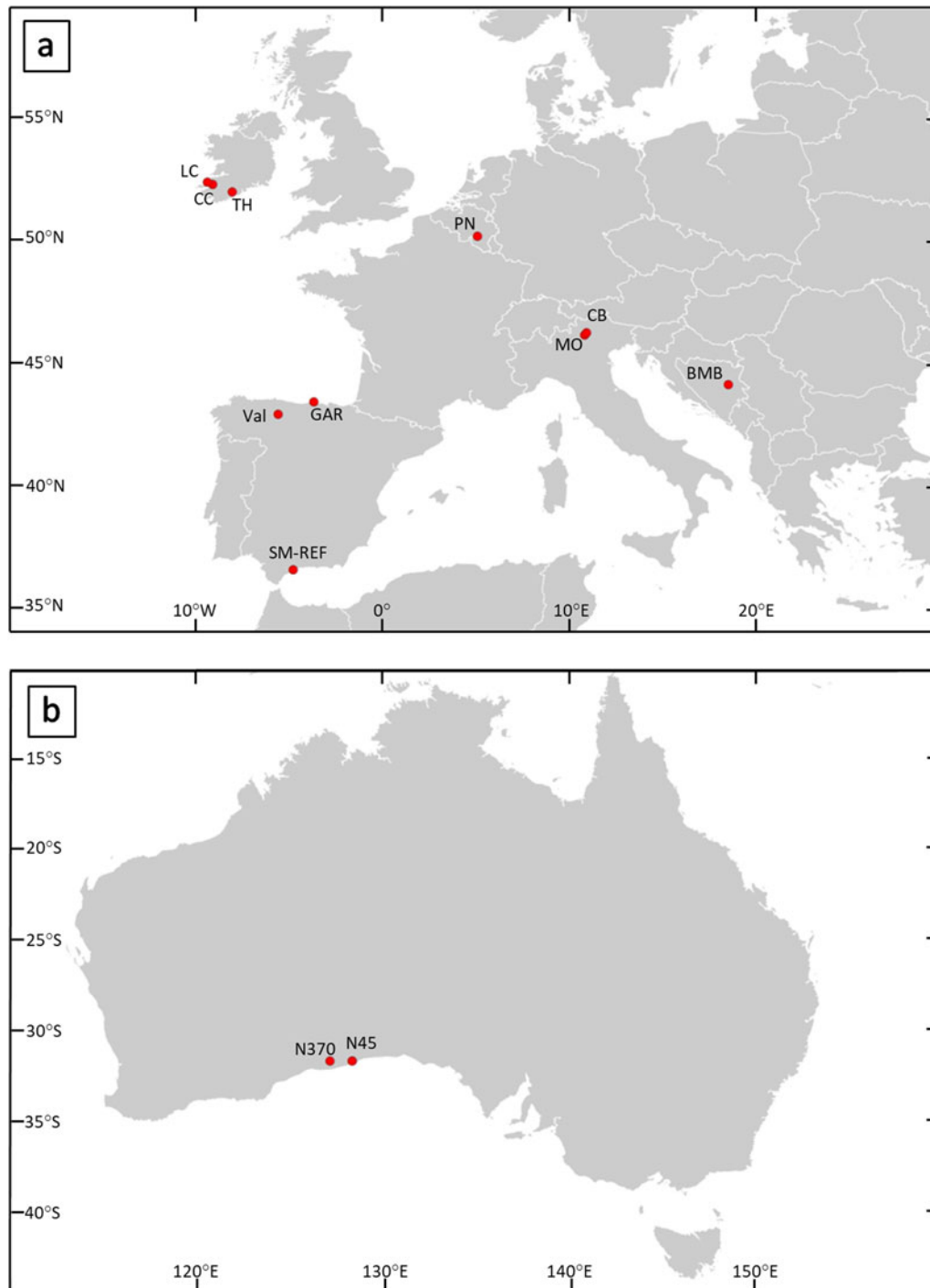
Figure 1. Map of sampling sites in Europe (**a**) and Australia (**b**). Labels refer to (**a**) the letters in the sample name and (**b**) the cave number. See Table 1.

carbonate structure. By contrast, in this study, the source of ^{36}Cl of interest is atmospherically produced (known as meteoric ^{36}Cl) that it is rapidly produced in the atmosphere by GCR bombardment of ^{40}Ar and is transported to Earth's surface in precipitation (e.g., rainfall) and can reflect high-frequency solar irradiance fluctuations. The meteoric component is often thought to be only loosely bound to the rock, and in studies interested in the in situ–produced component, the meteoric fraction is routinely removed by leaching crushed samples in deionised water before the in situ–produced ^{36}Cl is extracted by complete dissolution of the carbonate

(Phillips et al., 1986). For this reason, a water-leaching method would preferentially extract the loosely bound meteoric ^{36}Cl.

To measure ^{36}Cl/Cl ratios, sufficient Cl (at least 2 mg at the time of measurement) had to be extracted from the carbonate to form AgCl targets for AMS analysis at the PRIME Laboratory, Purdue, USA. Large speleothem samples (0.1–1.1 kg) were broken using a jaw crusher and then pulverised in a clean agate ball mill and leached in deionised water. The supernatant was spiked with a calibrated ^{35}Cl-enriched ^{35}Cl/^{37}Cl spike (Oak Ridge Laboratories, USA). Cl was concentrated onto preconditioned ion-exchange

Table 1. Speleothem samples, cave locations, climate settings, and analyses carried out in this study.

Sample name	Cave, location	Lat. (°)	Long. (°)	Alt. (m asl)	Distance from coast (km)	Köppen–Geiger climate classification[a]	Form	Analyses[b]	Reference
LC1	Lisodigue Cave, SW Ireland	52.3	−9.8	35	3	Cfb	Stalagmite	Fabric, leach, INAA	Coleman (1965)
LC5	Lisodigue Cave, SW Ireland	52.3	−9.8	35	3	Cfb	Stalagmite	Fabric, leach, INAA	Coleman (1965)
PN5	Pere Noël, SE Belgium	50.1	5.2	180	200	Cfb	Stalagmite	Fabric, leach, INAA	Verheyden et al. (2000); Fairchild et al. (2001)
PN6	Pere Noël, SE Belgium	50.1	5.2	180	200	Cfb	Stalagmite	Fabric, leach, INAA	Verheyden et al. (2000); Fairchild et al. (2001)
CB25	Cesare Battisti Cave, NE Italy	46.2	11	1880	130	Dfb	Flowstone	Fabric, leach, INAA	Johnston et al. (2018)
CB41	Cesare Battisti Cave, NE Italy	46.2	11	1880	130	Dfb	Flowstone	Fabric, leach, INAA, ^{36}Cl/Cl	Johnston et al. (2018)
SM-REF-02	El Refugio Cave, S Spain	36.6	−4.7	620	10	Csa	Stalagmite	Fabric, leach, INAA	Baldini et al. (2019)
Val-01	Valporquero Cave, N Spain	42.9	−5.6	1334	70	Csb	Stalagmite[c]	Fabric, leach, INAA	Duran et al. (2000)
CC4	Crag Cave, SW Ireland	52.2	−9.5	60	25	Cfb	Stalagmite	Leach, INAA	McDermott et al. (1999); Fairchild et al. (2001)
GAR-02	La Garma Cave, N Spain	43.4	−3.7	80	7	Cfb	Stalagmite	Leach, INAA	Jackson (2009)
CCSiteB	Crag Cave, SW Ireland	52.2	−9.5	60	25	Cfb	Bedrock	Leach, INAA	Tooth and Fairchild (2003)
MO7	Moline Cave, Trentino, NE Italy	46.1	10.9	680	140	Dfb	Stalagmite	Fabric, μXRF	Johnston et al. (2013)
FM13	Matilda Cave 6N-370, Nullarbor, S Australia	−31.8	127.8	100	40	Bwk	Stalagmite	Fabric, μXRF	Woodhead et al. (2019)
FS04	Winbirra Cave 6N-45, Nullarbor, S Australia	−31.8	128.4	92	15	Bwk	Stalagmite	Fabric, μXRF	Webb and James (2006)
MO1	Winbirra Cave 6N-45, Nullarbor, S Australia	−31.8	128.4	92	15	Bwk	Stalagmite	Fabric, μXRF	Webb and James (2006)
TH1	Temple Hill/Beaumont Caves, Cork, S Ireland	51.9	−8.4	20	15	Cfb	Flowstone	^{36}Cl/Cl	Oldham (1981)
BMB04	Bijambare Cave, Bosnia and Herzegovina	44.1	18.5	960	150	Dfb	Stalactite	^{36}Cl/Cl	Milanolo and Gabrovšek (2009, 2015)
BMB06	Bijambare Cave, Bosnia and Herzegovina	44.1	18.5	960	150	Dfb	Stalactite	^{36}Cl/Cl	Milanolo and Gabrovšek (2009, 2015)

[a]Köppen–Geiger climate classification based on data from Beck et al. (2018).
[b]μXRF = micro X-ray fluorescence; INAA = instrumental neutron activation analysis.
[c]Aragonite composition.

Table 2. Cl concentrations and fabrics of various speleothems analysed in this study.

| Sample | Water leaching | | INAA | | Fabric | |
	Sample weight (g)	Cl⁻ conc.[a] (mg/kg)	Sample weight (g)	Cl⁻ conc.[b] (mg/kg)	Group	Description
LC1	10.35	3.2 ± 0.2	3.70	4.7 ± 1.3	1	Laminated micrite, microsparite, sparite (columnar microcrystalline type, compact, translucent)
LC5	12.56	3.2 ± 0.2	5.11	13.0 ± 2.1	2	Laminated, micrite, microsparite sparite (columnar microcrystalline type), porous
PN5	9.78	1.2 ± 0.1	1.36	<8	1	Columnar, interlocking mosaic
PN6	10.84	1.5 ± 0.1	6.22	3.0 ± 1.2	1	Columnar, microcrystalline type (porous?), interlocking mosaic
CB25	10.06	5.7 ± 0.3	3.91	5.3 ± 0.8	3	Dendritic, porous
CB41	10.49	6.2 ± 0.3	2.52	14.0 ± 1.7	2	Laminated micrite, sparite (columnar), microsparite; detritus-rich porous; arranged in "botryoidal" morphologies
SM-REF-02	9.90	2.6 ± 0.1	5.77	3.1 ± 0.9	3	Dendritic/micrite
Val-01	10.25	2.3 ± 0.1	2.10	7.1 ± 0.9	4	Aragonite, acicular fans (porous)/rays
CC4	10.63	1.5 ± 0.1	2.00	<3	1	Columnar (compact?)[c]
GAR-02	10.05	3.8 ± 0.2	1.91	6.0 ± 1.0	3	Laminated columnar/dendritic[c]
CCSiteB	10.66	13 ± 0.7	1.20	23 ± 5.8		Lower Carboniferous limestone

[a]Uncertainties are stated at 5%.
[b]Instrumental neutron activation analysis (INAA) uncertainties are quoted to 1σ.
[c]Fabric identified from hand-specimen only.

columns (AG 1-X8, 100–200 mesh resin). The column containing the sample was rinsed with 0.1 M NH_4OH, and then 0.05 M HNO_3. The Cl was eluted with 0.15 M HNO_3, the solution was collected, and 1 M $AgNO_3$ and concentrated HNO_3 were added to form AgCl precipitate. This was centrifuged, and the supernatant was removed. NH_4OH was used to dissolve the AgCl, $Ba(NO_3)_2$ solution was added to remove SO_4^{2-}, and this was followed by reprecipitation of the purified AgCl by addition of HNO_3; this purification sequence was repeated several times. $^{35}Cl/^{37}Cl$ ratios in spiked samples were used to calculate leachable Cl concentrations by isotope dilution (ID-) AMS (Table 3). $^{36}Cl/Cl$ ratio measurements of pure NaCl samples taken directly from the underground mine face of the Irish Salt Mining and Exploration Company (Northern Ireland) yielded an average value of $15.96 \pm 4.55 \times 10^{-15}$ (n = 3), a value that intrinsically includes background interferences during target preparation and has been accounted for as part of the spike correction.

RESULTS

Speleothem fabrics

The selected speleothems covered a wide range of fabrics (Figs. 2 and 3), with the laminated specimens being characterised by complex fabric-type relationships. Consequently, in the descriptions provided in Table 2, fabrics have been grouped according to the most prominent type classified by Frisia (2015) and revised for the columnar types by Frisia et al. (2022). The following groups have been defined:

Fabric group 1—typical of LC1, PN5, PN6, CC4, FS04, FM13, and MO1—consists of predominant columnar compact, elongated columnar, and columnar open (FM13 and MO1; Fig. 3), associated with micrite layers (in FS04; Fig. 3) and columnar microcrystalline type in the laminated LC1, PN5, PN6 (Fig. 2a, c, and d), and CC4 samples.

Fabric group 2—typical of LC5 and CB41 (Fig. 2b and f)—consists of predominant columnar microcrystalline type associated with columnar porous layers (cf. Frisia et al., 2022), micrite laminae, and microsparite. The microsparite fabric is more common in CB41 than in LC5 and appears to crosscut through several columnar microcrystalline and micrite laminae (Fig. 2f). In CB41, some micrite forms clots similar to the clotted peloidal micrite microfabric observed in microbialites (cf. Della Porta, 2015). CB41 also shows void-filling cements that are commonly interpreted as the result of dissolution–reprecipitation. All speleothems in fabric group 2 are characterised by pervasive intercrystalline (and some intracrystalline) porosity.

Fabric group 3—typical of CB25, SM-REF-02 (Fig. 2e and g), and GAR-02 —is predominantly dendritic. In SM-REF-02, micrite is associated with the dendritic fabric and seems to form clotted microfabrics. Fabric group 3 is characterised by pervasive intercrystalline porosity, with millimetre-scale pores showing crosscutting relationships with the layers, rounded morphologies, and micrite coatings at the bottom that suggest their origin through postdepositional dissolution processes.

Fabric group 4—typical of stalagmite Val-01 (Fig. 2h)—consists of very elongated, aragonite needles, with some evidence of interneedle crystal cementation by mosaic calcite and, possibly, micritisation of the outer needle surface (cf. Martín-García et al., 2009). Although there is no clear evidence for diagenesis, micritisation may point to postdepositional transformation.

Cl concentrations

Figure 4 compares the Cl concentrations measured using the two different techniques (water leaching and INAA) simultaneously,

Table 3. Speleothem Cl⁻ concentrations, ^{36}Cl/Cl ratios, ^{36}Cl concentrations, and chemical processing parameters.

Sample name	Cave, location	Age	Mass calcite (g)	Cl⁻ from sample (%)[a]	Cl conc. (mg/kg) ID-AMS[b]	Measured		Spike-corrected present day		Spike-corrected initial value[c]		Local rainfall
						^{36}Cl/Cl ratio (× 10⁻¹⁵)	^{36}Cl conc. (atoms/kg) (× 10⁶)	^{36}Cl/Cl ratio (× 10⁻¹⁵)	^{36}Cl Conc. (atoms/kg) (× 10⁶)	^{36}Cl/Cl ratio (× 10⁻¹⁵)	^{36}Cl Conc. (atoms/kg) (× 10⁶)	^{36}Cl/Cl ratio (× 10⁻¹⁵)[d]
Flowstones												
CB41	Cesare Battisti, NE Italy	124 ± 4 ka[e]	102	33.9	9.24 ± 0.07	105 ± 20	16.5 ± 3.2	74 ± 25	11.6 ± 4.0	98 ± 34	15.4 ± 0.5	202 ± 27
TH1	Temple Hill Cave, S Ireland	Holocene[f]	271	32.7	2.39 ± 0.03	69 ± 8	2.8 ± 0.3	36 ± 11	1.4 ± 0.4	36 ± 11	1.4 ± 0.4	60 ± 4
Stalactites												
BMB04	Bijambare Cave, Bosnia and Herzegovina	3165 ± 35 ^{14}C yr BP[g]	1071	51.6	1.20 ± 0.01	53 ± 10	1.1 ± 0.2	39 ± 14	0.8 ± 0.3	40 ± 15	0.8 ± 0.3	128 ± 19
BMB06	Bijambare Cave, Bosnia and Herzegovina	3165 ± 35 ^{14}C yr BP[g]	1139	51.8	1.27 ± 0.01	90 ± 8	1.9 ± 0.2	74 ± 23	1.6 ± 0.5	75 ± 24	1.6 ± 0.5	128 ± 19

[a]Additional Cl was derived from the spike.
[b]ID-AMS, isotope dilution accelerator mass spectrometry.
[c]^{36}Cl radioactive decay correction ($\lambda = 2.303 \times 10^{-6}$/yr).
[d]From Johnston and McDermott (2008).
[e]Based on the ages of coeval speleothems in the same cave (Johnston et al., 2018)
[f]Preliminary U-series analyses suffered from high ^{230}Th backgrounds, but the results indicated a Holocene age.
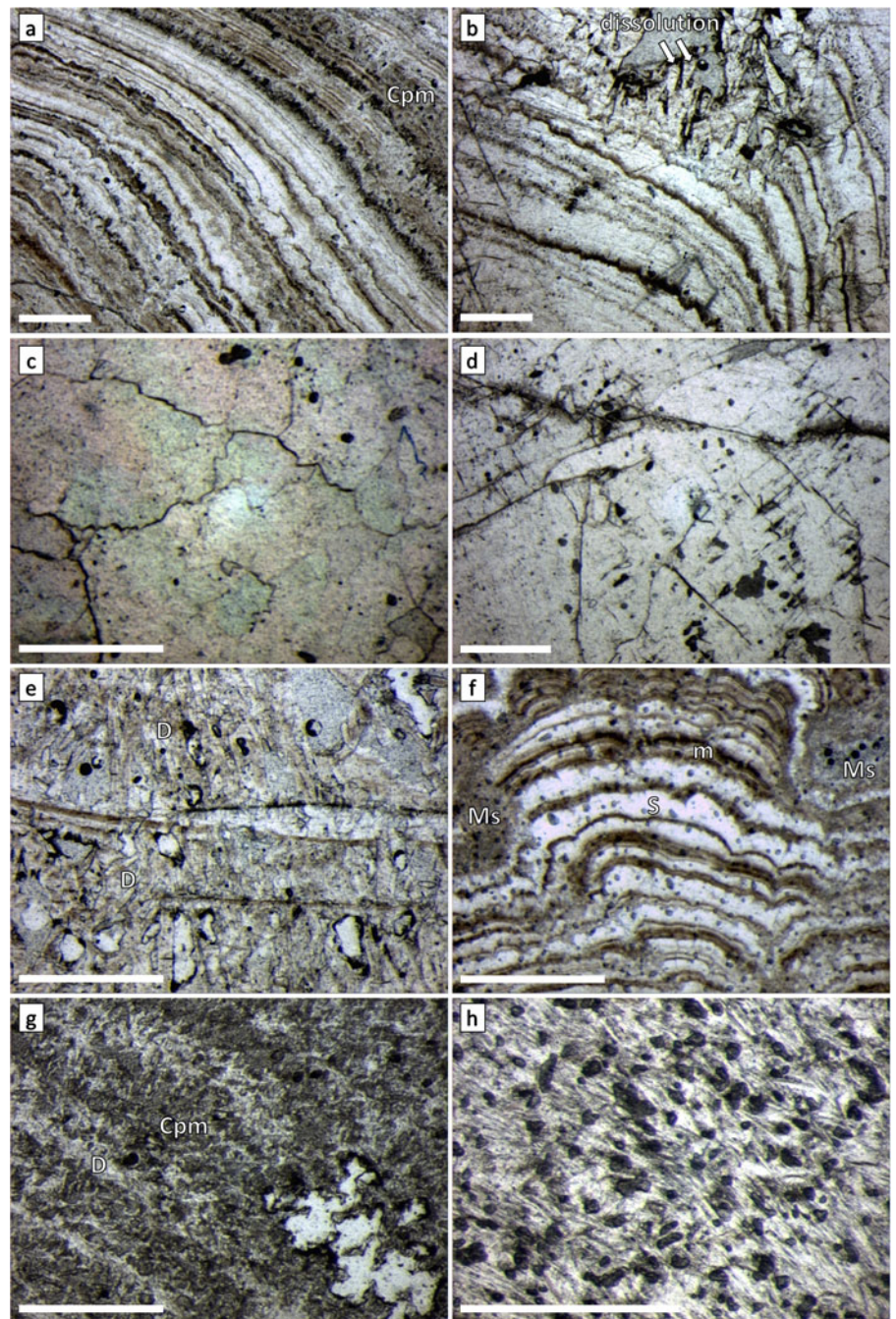[g]Preliminary raw ^{14}C date of nearby stalagmite.

Figure 2. Optical microscopy images to show fabrics of selected speleothems analysed for chlorine concentration. (**a**) LC1 from Lisodigue Cave, SW Ireland; (**b**) LC5 from Lisodigue Cave, SW Ireland; (**c**) PN5 from Pere Noël, SE Belgium; (**d**) PN6 from Pere Noël, SE Belgium; (**e**) CB25 from Cesare Battisti Cave, NE Italy; (**f**) CB41 from Cesare Battisti Cave, NE Italy; (**g**) SM-REF-02 from El Refugio Cave, S Spain; (**h**) Val-01 from Valporquero Cave, N Spain. Cpm, clotted peloidal micrite; D, dendritic fabric; m, micrite; Ms, microsparite; S, sparite. Scale bars: 1 mm. All images are in parallel polars.

colour/symbol coded based on the fabric groups of the analysed speleothems. The water-soluble Cl⁻ concentrations in the selected speleothems ranged from 1.2 to 6.2 mg/kg (mg Cl/kg carbonate), while total Cl concentrations were between 3 and 14 mg/kg (Fig. 4a, Table 2). Of note, pairs of speleothem samples from the same cave measured in this study (LC1 and LC5; PN5 and PN6; CB25 and CB41) exhibit similar water-soluble Cl⁻ concentrations, although their total Cl concentrations vary (Table 2). The proportion of water-soluble Cl⁻ as a percent of the total Cl (Fig. 4b) shows that the water-leaching method typically yields around half of the total Cl in these speleothem samples (average yield was 53%, ranging from 25% to essentially all the Cl). These results are consistent with our idea that the two different measurement techniques target different components of the total

Cl contained within the speleothems (i.e., the water-soluble Cl⁻ comprises only a fraction of the total Cl). Importantly, Figure 4b shows that the proportion of water-soluble Cl⁻ is greater (>50%) in samples from fabric groups 1 and 3 than that from fabric groups 2 and 4 (<50%). Following the premise that the water-soluble Cl⁻ fraction is made up solely of fluid inclusions, Figure 5 shows the theoretical percentage of fluid inclusions that a calcite speleothem would require, at various Cl⁻ concentrations, to gain the water-soluble Cl⁻ fraction extracted from the samples analysed here. Taking fluid inclusion water—equivalent to that of the drip water—with a Cl⁻ concentration of, for example, 40 mg/L, to gain speleothem water-soluble Cl⁻ concentrations within the range measured here, the weight percent of the speleothem that would need to be composed of fluid inclusions should be between
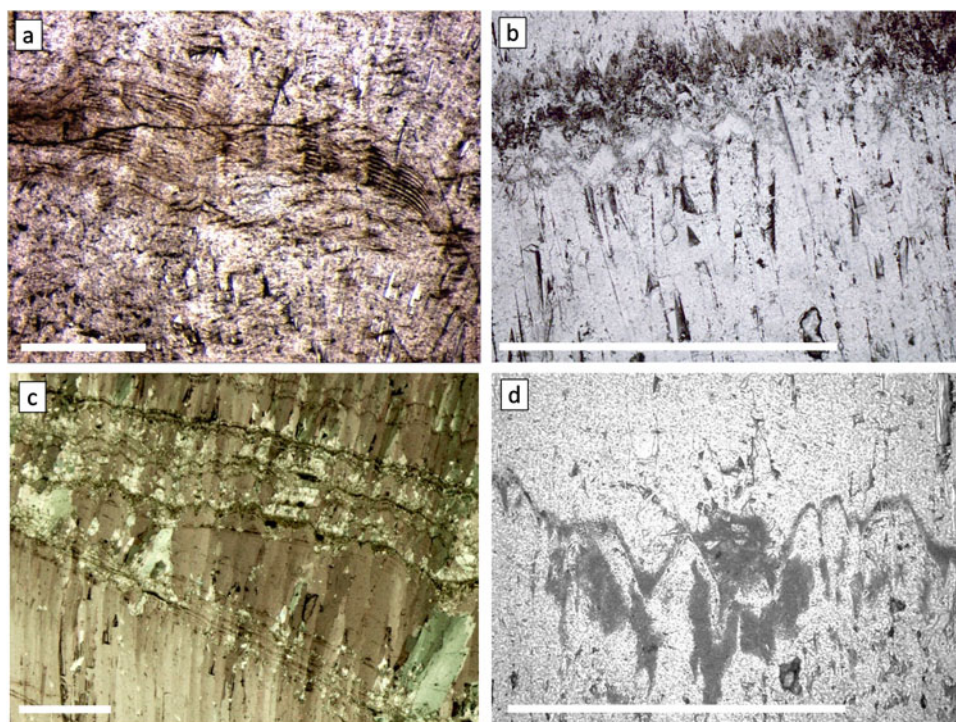
Figure 3. Optical microscope images to show fabrics of selected speleothems analysed also by synchrotron radiation micro X-ray fluorescence (μ-XRF). (**a**) MO7 from Moline Cave, Trentino, NE Italy; (**b**) FM13 from Matilda Cave 6N-370, Nullarbor, S Australia; (**c**) FS04 from Winbirra Cave 6N-45, Nullarbor, S Australia; (**d**) MO1 from Winbirra Cave 6N-45, Nullarbor, S Australia. Scale bars: 1 mm.

3% and 15% (Fig. 5a). However, to express this in a way that can be visually imagined, a calculation of the percentage of fluid inclusions required to gain the measured water-soluble Cl⁻ concentrations is plotted in terms of volume of the speleothem, taking into account the specific gravities of water and calcite (Fig. 5b). Again, taking, for example, a fluid inclusion water Cl⁻ concentration of 40 mg/L, the volume of a speleothem sample that would need to be composed of fluid inclusions to gain the values measured in our samples should be between 6% and 30% (Fig. 5b).

The Mississippian limestone bedrock from Crag Cave, SW Ireland, (CC SiteB; Table 2) yielded a total Cl concentration of 23 ± 5.8 mg/kg. This is a carbonate formation that likely consisted of biominerals or bio-induced minerals (mud mounds) (cf. Gallagher and Somerville, 1997) and thus represents high Cl and high Na (marine) parent waters and biomediated end-members. The Cl concentration of CC SiteB is in agreement with other carbonate rocks; for example, from Tioga Pass (6.2–38.7 mg/kg) and Gull Lake (23.5–30.5 mg/kg), both in Sierra Nevada (Stone et al., 1996), from an unweathered cave ceiling of Golgotha Cave, SW Australia (24 mg/kg) (Campbell et al., 2023), and in the Lower Jurassic Calcari Grigi limestone that forms the host rock of Cesare Battisti Cave (13.9 ± 2.9 mg/kg) (Ivy-Ochs et al., 2017) that contains our samples CB25 and CB41.

μ-XRF trace element maps

Synchrotron μ-XRF offers one of the few means of high-resolution mapping of elements lighter than Ca. High-resolution trace element maps are shown from four speleothems; sample MO7 from Moline Cave in Trentino, NE Italy, permits a detailed look at the Cl distribution in a relatively typical subalpine stalagmite (Fig. 6), while three samples from caves in the Nullarbor,

Australia (FM13, FS04, and MO1), allow the analyses of more unusual speleothems, with presumably high-Cl concentrations, to investigate, specifically, the incorporation of Cl related to detrital/biogenic impurities (Figs. 7–9). The Australian Nullarbor speleothems have been studied extensively, as they represent important archives of Pliocene climate, having a median age of 4.2 Ma (Sniderman et al., 2016; Woodhead et al., 2019). They are commonly characterised by layers of elongated, translucent columnar calcite that may be interrupted by P-rich micrite, which was interpreted as indicative of periodic colonisation of the speleothem surface by microbes (Frisia et al., 2012). In all μ-XRF trace element maps shown here (Figs. 6–9), Mg and often S show the outlines of crystals and the morphologies of crystal terminations. As for Si, its presence may be associated with microbial activity (Polyak and Güven, 2004; Johnston et al., 2021), but when Si is associated with Al, such association suggests both authigenic clay formation and presence of detrital silicate particulate (Frisia et al., 2012). The distribution of Cl, compared with the other elements, varies substantially. In MO7, Cl is distributed in discrete spots, similar to those of Na and S, while it is mostly not related with Al and Si (Fig. 6). FM13 shows columnar crystal tips that seem to be "corroded" between deposition of successive open columnar layers (Figs. 3b and 7) and may mark a change in the environment of deposition. Here, Cl is anti-correlated with Na, Mg, S, and Sr, and only slightly seen in some grains containing Al, Si, and P (Fig. 7). In FS04, Cl concentration distribution follows crystal tips and is associated with Si, but again an anti-correlation with Na is apparent (Fig. 8). Critically, in MO1 (Fig. 9), Cl is distributed over the entire mapped area as discrete spots correlating with Na, but it has a secondary relationship with Si, Al, and micritisation (cf. Frisia et al., 2012).
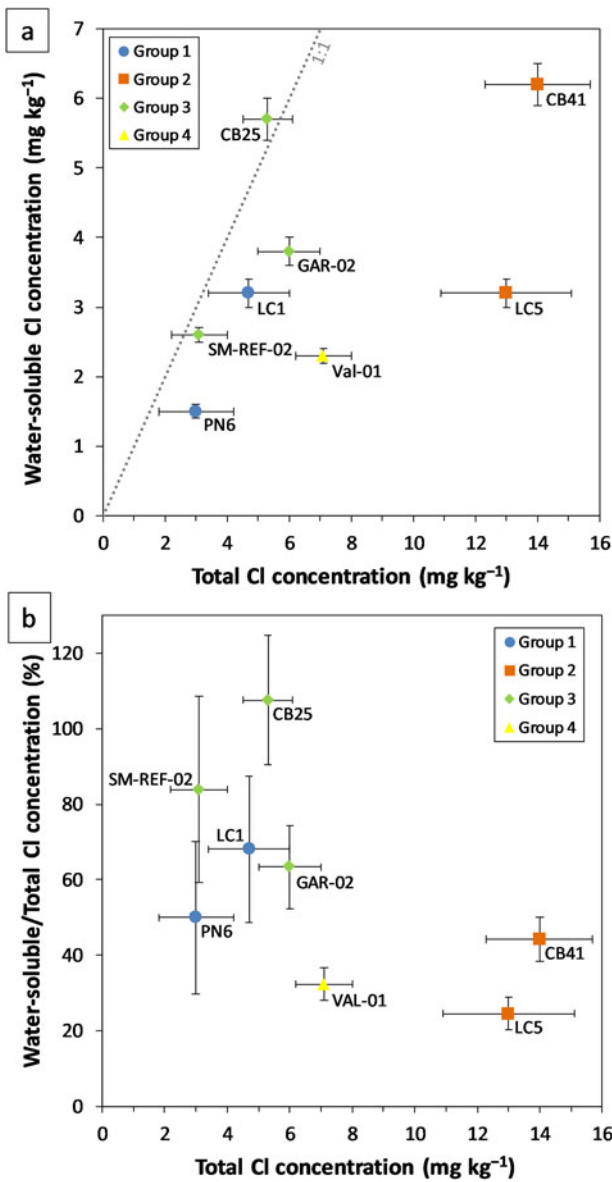
Figure 4. Comparison of water-soluble and total Cl concentrations derived using two different analytical techniques, coded by fabric. (**a**) Total Cl concentrations measured by instrumental neutron activation analysis (INAA) plotted against water-soluble Cl⁻ concentrations obtained by the water-leaching method. (**b**) Total Cl concentrations measured by INAA against the percentage of water-soluble Cl⁻ of the total Cl concentration. Fabric codes can be highly summarised as (see Table 2 and "Results" for full details): (1) compact columnar (blue circles), (2) microsparite with intercrystalline porosity and micrite laminae (orange squares), (3) laminated and dendritic with intercrystalline porosity (green diamonds), (4) aragonite needles (yellow triangle).
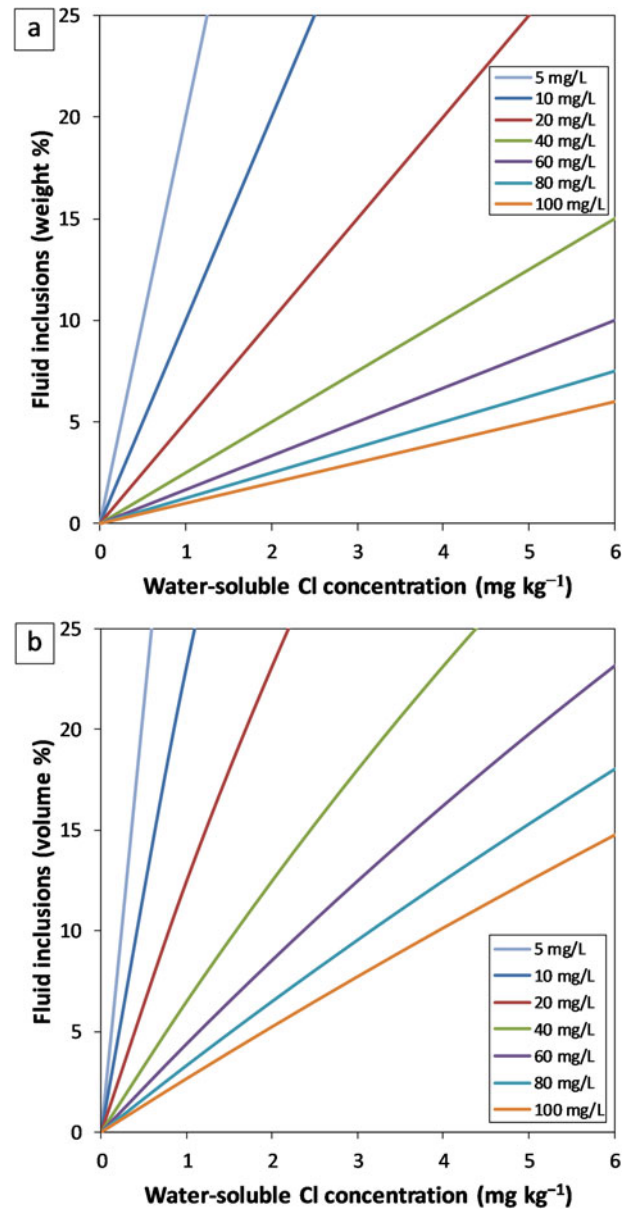

Figure 5. Theoretical calculations of the percentage of a speleothem sample that would be required to be composed of fluid inclusions to gain water-soluble Cl⁻ at concentrations typical of the speleothems analysed in this study, for different fluid inclusion water Cl⁻ concentrations, reported as weight % (**a**) and volume % (**b**).

$^{36}Cl/Cl$ ratios in speleothems

Table 3 shows the results of the first measurements of the ^{36}Cl/Cl ratio on speleothem samples; including two flowstone samples and two stalactites. The measured ^{36}Cl/Cl ratios and ^{36}Cl concentrations have been corrected for the addition of an enriched spike to give the spike corrected value at the time of measurement (present day). Because ^{36}Cl is radioactive, the values needed to undergo a correction for the radioactive decay that has occurred since deposition, based on the ^{36}Cl decay rate ($\lambda = 2.303 \times 10^{-6}$/ yr) and the age of the sample, to give an "initial" value. Given the long half-life of ^{36}Cl (301,300 ± 1,500 yr), for younger

(Holocene) samples, this correction to gain the initial value is minor (Table 3) and well within the uncertainties of the age-uncorrected value. For older samples, however, this correction becomes significant, as shown in the example of CB41 (Table 3), where the age-uncorrected (i.e., at the time of measurement) ^{36}Cl/ Cl ratio of 74×10^{-15} is corrected to an initial value (i.e., at the time of deposition) of 98×10^{-15} based on an age of 124 ka. Unfortunately, our attempts at dating CB41 were hampered by a very low ^{230}Th/^{232}Th activity ratio; hence, a large detrital correction would be needed, giving unacceptable uncertainties. Therefore, here, the age had to be estimated based on the U-series ages of three coeval speleothems deposited in the same cave that have been shown to form only during interglacial conditions, so we can be relatively confident that CB41 also formed
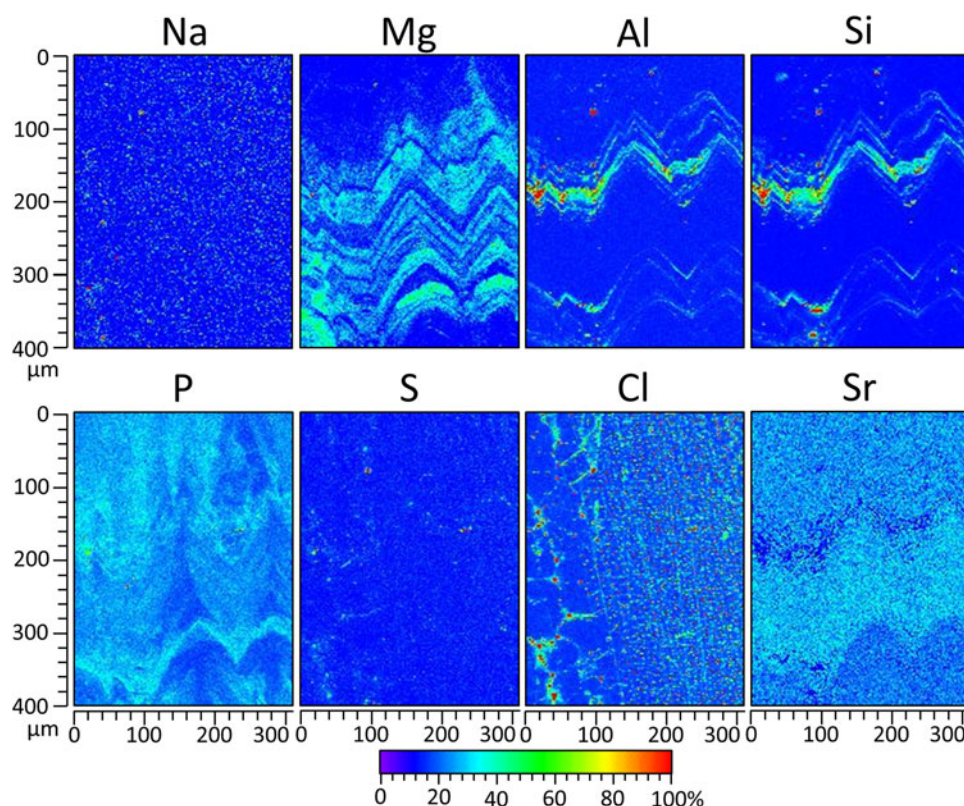
Figure 6. Synchrotron radiation micro X-ray fluorescence (μ-XRF) maps of sample MO7 from Moline Cave, Trentino, NE Italy. The maps show the distribution of concentrations of Na, Mg, Al, Si, P, S, Cl, and Sr.

in the same time window around 124 ± 4 ka (Johnston et al, 2018). Because this is a pilot study, and due to the large sample sizes required, our $^{36}Cl/Cl$ ratio measurements were carried out on the material available to us at the time; future attempts at these measurements should select speleothems that have already been accurately dated.

DISCUSSION

Here, we test the hypothesis that Cl concentrations in speleothems are directly correlated with the Cl^- content of the feeding drip waters; a situation that would permit speleothem Cl to be used as a proxy for palaeo-precipitation or evapotranspiration, and thus to be used to infer the climate setting. Theoretically, due to its strongly hydrophilic nature, Cl^- could be considered to travel quickly and conservatively though the vadose zone, albeit in the absence of anthropogenic sources, such as road salt (e.g., Münsterer et al., 2012), highly-soluble Cl-rich minerals in the catchment area, or interactions with soil and vegetation (e.g., Cornett et al., 1997; Milton et al., 2003; Bastviken et al., 2007; Treble et al., 2016). Because rainwater Cl^- concentrations depend strongly on the distance from the coast, one could expect cave drip-water Cl^- concentrations, and thus speleothem Cl concentrations, to correlate with the distance from the coast. Our limited data from cave sites studied here show that Cl^- concentrations in drip waters are indeed higher in the coastal sites (Crag Cave and La Garma Cave, 12–43 mg/L and 14–137 mg/L, respectively) than inland (Cesare Battisti Cave, ca. 0.5 mg/L; Borsato et al., 2016). However, our speleothem data do not reflect this trend. For example, speleothem LC1 from a coastal site had a low total Cl

concentration of 5 mg/kg, while inland CB41 had a higher Cl concentration of 14 mg/kg (Tables 1 and 2). Alternatively, evapotranspiration could elevate Cl^- concentrations in drip waters from more arid regions, and consequently in the speleothems as well. However, our results show the opposite. For example, low Cl concentrations (3.1 mg/kg) characterise speleothem SM-REF-02 from southern Spain, which endures a strong summer water deficit (Köppen–Geiger climate classification: Csa; Beck et al., 2018), whilst high Cl concentrations were detected in the subalpine CB41 flowstone (Dfb). Overall, our data indicate that speleothem Cl concentrations do not correspond with drip-water Cl^- concentrations (i.e., the Cl^- signal in the drip water is not transferred to the speleothem). This implies that Cl in speleothems is not a straightforward proxy of climate. Accordingly, the transfer of Cl^- from the drip water into the speleothem carbonate requires investigation.

Fabrics and Cl incorporation

In an attempt to understand how Cl is incorporated into our studied speleothems, we compared their Cl concentrations, measured with the different methods, with their fabrics. Considering the results of the water-leaching method (Fig. 4a, Table 2), it is clear that pairs of samples from the same caves have similar Cl^- concentrations. This is in contrast to the results of total Cl (measured by INAA), in which pairs of samples from the same caves show large differences in their Cl concentrations. For example, LC1 and LC5 have identical water-soluble Cl^- concentrations of 3.2 ± 0.2 mg/kg but significantly different total Cl concentrations of 5 mg/kg and 13 mg/kg, respectively. Accordingly, we
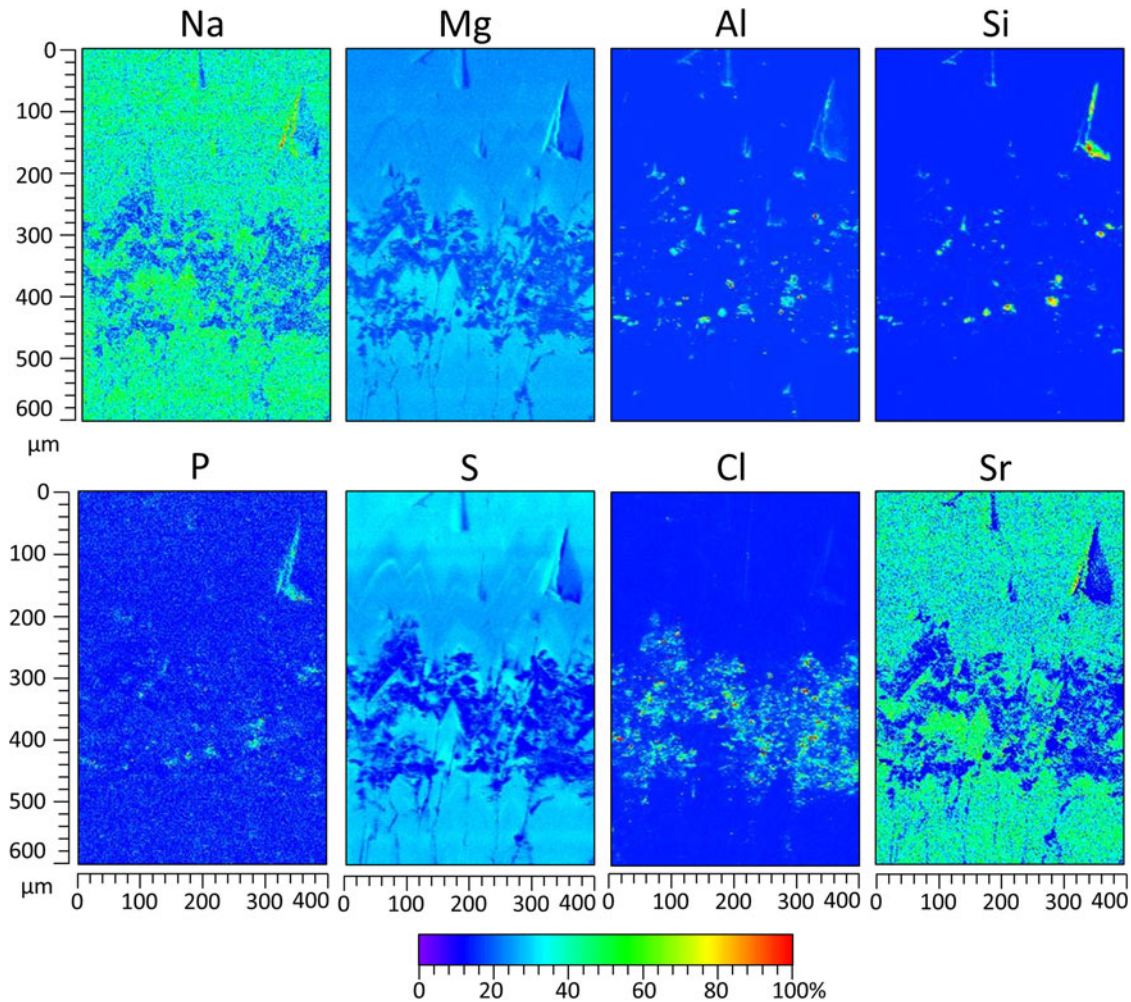
Figure 7. Synchrotron radiation micro X-ray fluorescence (μ-XRF) maps of sample FM13 from Matilda Cave 6N-370, Nullarbor, S Australia. The maps show the distribution of concentrations of Na, Mg, Al, Si, P, S, Cl, and Sr.

propose the concept of two fractions of Cl within speleothems: (1) loosely bound and water soluble and (2) strongly bound and scarcely soluble to insoluble in water. The water-leaching method extracts only the water-soluble fraction, while INAA measures both fractions, as total Cl, where the strongly bound, insoluble fraction is the difference between the two measurement methods (i.e., the excess Cl in the INAA method). Every speleothem likely contains Cl derived from both fractions, but the proportions of these will vary (Fig. 4b). Given the similarity in water-leached Cl^- concentrations between pairs of speleothem samples from the same caves, the water-soluble, loosely bound Cl^- could possibly reflect environmental conditions, such as Cl^- concentration of drip waters, while the excess, strongly bound Cl may depend on individual speleothem properties, such as fabric and contents of inorganic and organic compounds.

The stalagmites from Lisodigue Cave are good candidates to interrogate how Cl may be incorporated in speleothems, as they are from the same cave and have similar ages, but some differences in fabrics (fabric group: LC1 = 1, LC5 = 2). In stalagmite LC1, the total Cl concentration is 4.7 mg/kg, whilst LC5 has a high Cl concentration of 13 mg/kg. LC1 preserves delicate primary features, such as clotted peloids consisting of micrite, and the fabric is overall more compact in LC1 (Fig. 2a) than in LC5

(Fig. 2b). The micrite defines very dark laminae, where it is likely that organic particulates were entrapped between crystals and where organic compounds may have influenced the formation of clotted peloids. LC5 has similar lamination, but it is more porous, with evidence of rounded micromorphologies and surfaces that crosscut several laminae, which are here interpreted as due to dissolution possibly associated with oxidation of organic compounds (Fig. 2b). Petrographic observations did not reveal the presence of clotted peloidal micrite, although this might be a localised difference due to where the thin section was obtained. Lamination is present in both LC1 and LC5 and is likely the result of annual flushing of the same organic and particulate matter into the cave system (cf. Borsato et al., 2007), where differences between the two samples are potentially caused by different dripwater pathways through the soil and bedrock. Thus, in addition to a contribution from fluid inclusions, incorporation of Cl into LC1 and LC5 might be a result of Cl association with organic compounds in the clotted peloidal micrite portion of the layers.

The lowest Cl concentrations, both water soluble and total, found in this study were in PN5 (water soluble = 1.2 mg/kg; total below detection limits) and PN6 (water soluble = 1.5 mg/kg; total = 3 mg/kg) (Table 2), which are also the speleothems with the most uniform fabric (fabric group 1) consisting of an
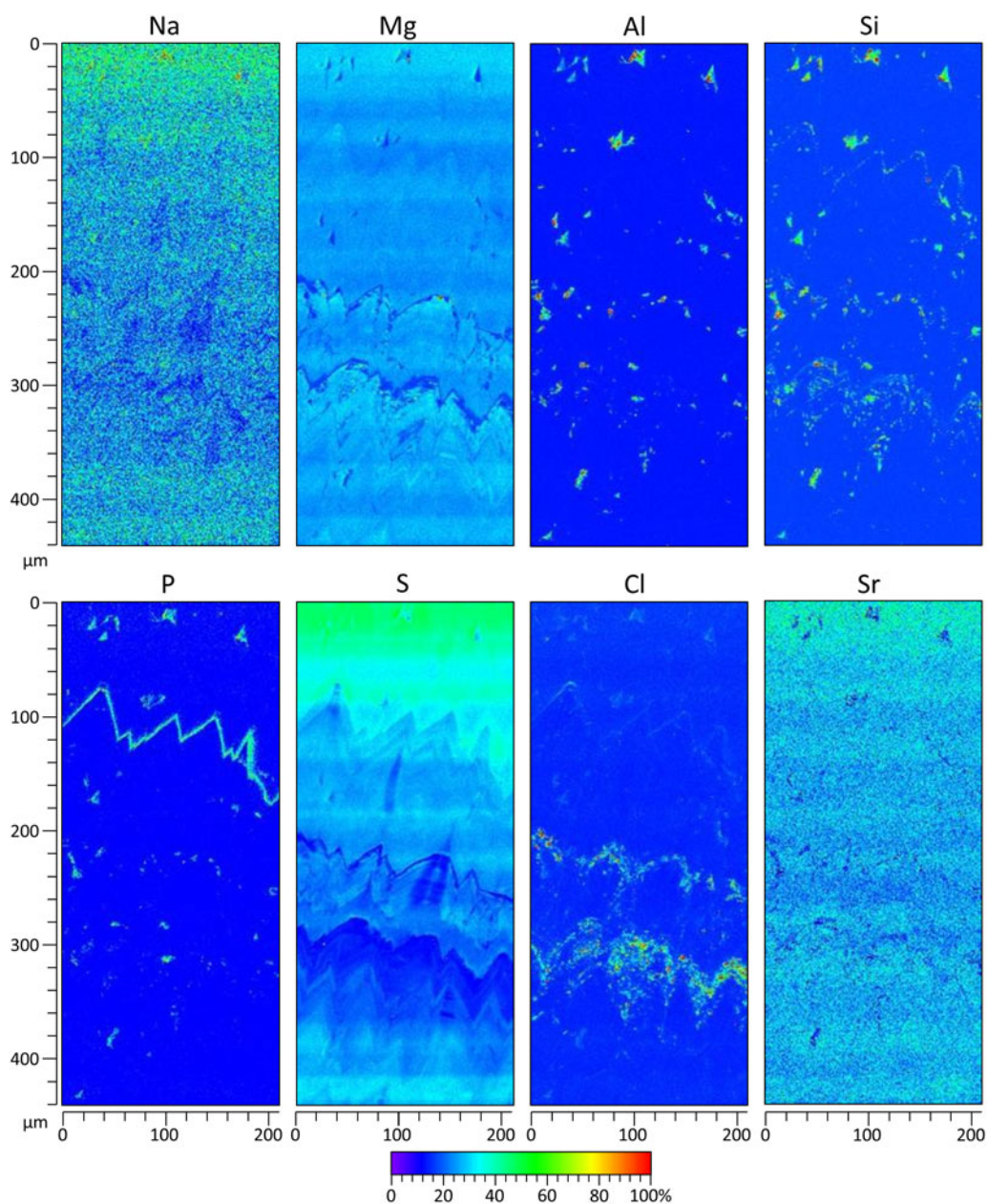
Figure 8. Synchrotron radiation micro X-ray fluorescence (μ-XRF) maps of sample FS04 from Winbirra Cave 6N-45, Nullarbor, S Australia. The maps show the distribution of concentrations of Na, Mg, Al, Si, P, S, Cl, and Sr.

interlocking mosaic of calcite crystals (Fig. 2c and d). This fabric was most commonly observed in speleothems in which some degree of diagenetic (here intended as an early, postdepositional process) modifications occurred (Frisia, 2015; Frisia et al., 2018). The PN speleothems contain a low proportion of particulate matter (Fig. 2c and d). Their compact fabrics leave little space for fluid inclusions, but they are characterised by intercrystalline porosity that could host water-soluble Cl^-.

Flowstone CB25 exhibits relatively high and comparable water-soluble and total Cl concentrations; 5.7 mg/kg and 5.3 mg/kg, respectively. CB25 predominantly displays an open dendritic (skeletal) fabric (fabric group 3) and high meso- to macroporosity (Fig. 2e). The branching framework and stepped crystal faces of this fabric result in pervasive microporosity, which would allow Cl^- to be hosted in fluid inclusions between pores or as relatively

soluble particulates at crystal steps/kinks. Furthermore, the dendritic fabric was shown to be characterised by crystal defects, such as lamellae and dislocations, which could perhaps incorporate Cl^-, possibly compensating for charge imbalances. The placement of CB25 on the 1:1 line between water-soluble and total Cl (Fig. 4a) indicates that practically all the Cl within this sample is loosely bound to the carbonate.

Flowstone CB41, from the same cave as CB25, has the highest Cl concentrations, both water soluble and total, of all the analysed suite of samples (Table 2). In the hand specimen, CB41 is characterised by high porosity, where pores are lined by isopachous cement or are completely filled by calcite. The sample also shows a high number of small fluid inclusions, in addition to macropores up to 3 mm in length, which likely host water-soluble Cl^-. However, given the low Cl^- concentrations of drip waters at
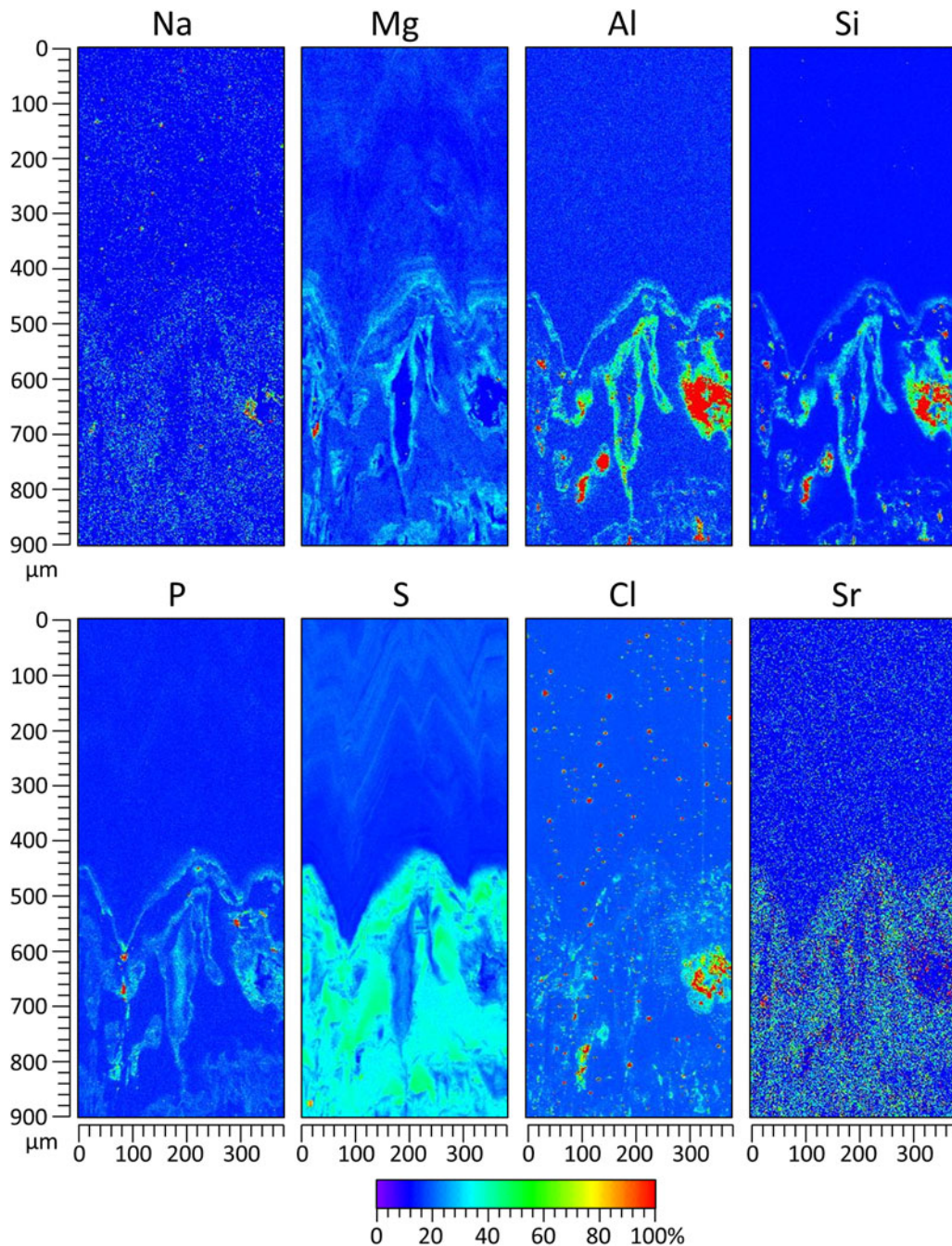
Figure 9. Synchrotron radiation micro X-ray fluorescence (μ-XRF) maps of sample MO1 from Winbirra Cave 6N-45, Nullarbor, S Australia. The maps show the distribution of concentrations of Na, Mg, Al, Si, P, S, Cl, and Sr.

this inland cave site, a second source of loosely bound Cl must be present. CB41 has a distinctive fabric (fabric group 2), consisting of laminae formed by micrite, which laterally pass into microsparite (Ms in Fig. 2f) and sparite arranged in botryoidal shapes (Fig. 2f). Some clotted peloidal micrite can be still observed, suggesting that the formation of micrite may have been bio-influenced. The fabrics have a distinctive peach colour—with the exception of white pore-lining and filling cements—that may be attributable to a high bulk sample Mn concentration (ca. 50−100 mg/kg). The presence of microsparite (Fig. 2f) indicates that CB41 may have undergone some early diagenesis. It then becomes plausible that its high water-soluble Cl⁻

concentration is the result of an input from Cl-bearing, diagenetic fluids, while the organic-rich micrite provides the strongly bound Cl component; these sources together then result in the high total Cl concentration observed.

Relative to the other speleothems, stalagmite SM-REF-02 (Fig. 2g) has a medium Cl concentration but, importantly, falls close to the 1:1 line between the Cl concentrations measured by leaching and by INAA (2.6 mg/kg and 3.1 mg/kg, respectively; Fig. 4a). This indicates that most of the Cl was loosely bound to the speleothem. The fabric is roughly laminated, composed of alternating dendritic and micritic fabrics, with some macro-porosity (fabric group 3). This could be interpreted as indicating

that a significant contribution of the Cl is hosted in fluid inclusions. Moreover, Cl is either particularly incompatible with the dendritic fabric or any Cl associated with dendritic crystals, perhaps, for example, nested in defect sites, is only loosely bound to the calcite and readily water soluble. Here, the micrite does not appear to contribute much to the total Cl composition. This disparity in Cl concentrations between speleothems that have similar fabric features (e.g., micrite content) suggests that the incorporation of other elements or organics not analysed in this study may affect Cl incorporation. Importantly, this highlights the complex processes that govern Cl concentrations in speleothems.

Stalagmite Val-01 is the only one entirely composed of aragonite and consists of an alternating fabric of rays and acicular fans, which leads to the appearance of compact and porous layers (Fig. 2h; fabric group 4). Val-01 has a low water-soluble Cl$^-$ concentration of 2.3 mg/kg but, relative to this, a total Cl concentration of 7.1 mg/kg. The alignment of the acicular crystals allows pores to develop at crystal terminations, trapping fluids that could contain Cl$^-$, accounting for some of the water-soluble Cl$^-$ fraction. However, the large nonsoluble component indicates that Cl could be incorporated bound to cations, such as Na$^+$ or K$^+$, or to organic compounds, in a mode that is unique to this aragonite fabric.

The differentiation between fabric groups and Cl concentrations in speleothems is clearly apparent in Figure 4. Fabric groups 1 and 3 fall close to the 1:1 line between total and water-soluble Cl concentrations (Fig. 4a), indicating that most of the Cl is held within the water-soluble and loosely bound fraction, supported in Figure 4b, which shows more than 50% of the Cl is from the water-soluble fraction. This is in contrast to fabric groups 2 and 4, which are farther from the 1:1 line between total Cl and water-soluble Cl$^-$ concentrations (Fig. 4a) and contain less than 50% of Cl derived from the water-soluble fraction (Fig. 4b), therefore indicating that fabric groups 2 and 4 have a mix of Cl sources, with a large proportion derived from the insoluble fraction. The most obvious source of water-soluble Cl$^-$ in speleothems is from fluid inclusions. Based on Figure 5, we theorise that to gain the concentrations of water-soluble Cl$^-$ found here, a large amount of fluid must be hosted within the speleothems (presuming the fluid inclusion solution retains the same Cl$^-$ concentrations as the feeding drip water). Speleothems are typically thought to contain about 0.1% (weight) of fluid inclusion water, ranging from approximately 0.05% to 0.5% (McDermott et al., 2005), corroborated by further estimates based on fluid inclusion isotope measurements on Hungarian speleothems that were found to contain about 0.1–0.2% (weight) fluid, with exceptional values up to ca. 0.6% (Demény et al., 2021). Consequently, using these estimates, the amount of fluid inclusion water required to provide the measured speleothem water-soluble Cl$^-$ fraction becomes implausible (Fig. 5a), implying either the solution trapped as fluid inclusions has a higher Cl$^-$ concentration than the drip water or there is another source(s) of water-soluble Cl$^-$ within speleothems. However, it has become apparent that the volume of water extracted from speleothems during fluid inclusion isotope analyses may be lower than that of the original speleothem, because water can escape through microfractures or evaporate during the analyses at a stage before the water is extracted (Fernandez et al., 2023), consequently, indicating that the calculated fluid inclusion content values (shown above) are underestimated. If fluid inclusion water is lost though evaporation, the Cl contained in the fluid inclusion water would be deposited as Cl salts within the porosity and thus would still contribute to the water-soluble Cl$^-$ fraction measured here. Indeed,

using internal 3D imaging, Shtober-Zisu et al. (2012) found the total porosity of certain speleothems to be <18% (volume), while the porosity varied between speleothems and also within the speleothems themselves due to differences in speleothem fabrics. Therefore, if this porosity still contains fluid inclusion water or was originally water filled and the fluid subsequently evaporated depositing water-soluble Cl salts, it could provide a large proportion of the water-soluble Cl$^-$ fraction at typical cave dripwater concentrations (Fig. 5b). Importantly, porosity was found to vary widely depending on the speleothem fabric (Shtober-Zisu et al., 2012), implying that speleothem fabric strongly influences the water-soluble Cl$^-$ concentrations.

Hence, our limited data show that speleothem fabrics are a factor in controlling the Cl concentrations of speleothem carbonate. The control of the fabrics encompasses the carbonate crystal shapes, the porosity, and the incorporation of particulate matter (including how these influence one another). This raises the question of whether fabrics and their associated micro and nano-scale growth defects play a role in the incorporation of other trace elements of palaeoclimatic significance into speleothems, which has only recently been given adequate consideration (Frisia et al., 2018, 2022).

μ-XRF trace element maps

μ-XRF mapping permits the visualisation of the distribution of trace elements at very high resolutions. Different trace elements can be associated with speleothem features, such as those elements that follow the crystal shapes and others that indicate inclusion of particulates. We now use more recently acquired μ-XRF maps of a suite of trace elements, including Cl, from a different set of well-characterised speleothems to offer further insights about Cl incorporation mechanisms in speleothems.

MO7 (Moline Cave, NE Italy)

In sample MO7 from Moline Cave, NE Italy, two different distributions of trace elements are apparent; the right-hand sides of the maps show well-defined crystal tips, notably on the Mg map, with high concentrations of Si and Al, likely as fine detrital particulates, following the crystal faces, while the left-hand sides show more disrupted crystal forms and accumulations of Si and Al in depressions (Fig. 6). The distribution of Cl also shows differences on either side of the map. On the right-hand side, Cl occurs as discrete spots that are similar to what is seen in the Na map, and thus, it is likely that the Cl is hosted in fluid inclusions (as NaCl in solution). Whereas, on the left-hand side of the map (Fig. 6), Cl is distributed along some sublinear features that cannot be attributed to associations with detrital particulates (Si and Al) or organic compounds (often associated with P; Frisia et al., 2012). The Cl has accumulated at nodes connecting these sublinear features, and these accumulations are also apparent in the Na and S maps, albeit not as visibly clear as in the Cl map. We therefore suggest that the Cl could be hosted within fluid inclusions that are distributed along microfractures or linear defects in the crystals. We interpret this to mean that, at least in the studied part of MO7, the majority of Cl is likely to be incorporated as part of the water-soluble and loosely bound fraction.

FM13 (Nullarbor)

In Nullarbor speleothem sample FM13 (Fig. 7), Cl appears to be concentrated in an area that has more disrupted crystals, as shown in Mg, S, and Sr distributions. The Cl distribution does not correlate directly with detrital material (Si and Al); however, the

disrupted zone does appear to have slightly more occurrences of Si and Al than other parts of the mapped area. The P distribution shows some faint similarities to those of Si and Al, potentially indicating that some of the particulates are related to organic compounds (cf. Frisia et al., 2012). Interestingly, there is an anti-correlation between Na and Cl, indicating that the Cl is unlikely to be hosted in fluid inclusions in the common form of NaCl. Critically, the data do not elucidate by what mechanism Cl was incorporated into FM13, but by process of elimination, we can suggest that Cl could be incorporated at crystal defect sites compensating for charge imbalances (but these are not associated with detrital material), as Cl containing minerals (combined with elements not analysed here), or as chlorinated organic compounds (that do not contain high concentrations of P and S).

FS04 (Nullarbor)

In Nullarbor speleothem sample FS04 (Fig. 8), the lower part of the synchrotron μ-XRF maps, particularly those of Mg and S, show morphologies of crystal terminations as rounded crystal tips, which suggests that dissolution may have occurred when crystals reached the surface of the water film. This phenomenon could reflect sporadic changes in environmental conditions causing percolation waters that were undersaturated with respect to calcite and low flow rates. The Cl is distributed along these layers, outlining the crystal tips, but this distribution is only vaguely reflected in the distribution of Si but not in Al, while Cl is anti-correlated with S. As in FM13, although vague, there appears to be some anticorrelation between Na and Cl, disputing the possibility of NaCl solution in fluid inclusions. Therefore, we cannot deduce the Cl incorporation mechanism for FS04, but again, as for FM13, we suggest the possibilities of crystal defect sites, other Cl-bearing minerals, or chlorinated organic compounds present in nano-scale inclusions.

MO1 (Nullarbor)

Nullarbor speleothem sample MO1, which mostly consists of translucent, elongated columnar calcite (Fig. 3d), shows a strong contrast between the upper and lower parts of the mapped area (Fig. 9). The lower part, with high concentrations of Mg, Al, Si, P, S, and Sr, has been previously interpreted as being associated with micrite (Frisia et al., 2012), while the upper part is cleaner calcite with low concentrations of those elements. The Cl map has some distinct features. In the lower part, a large, presumably detrital particle corresponding to high Al and Si concentrations, dominates the Cl map. Cl continues to follow a distribution similar to that of Al and Si in the lower part of the mapped area, pointing to Cl incorporation associated with detrital or particulate material, which may also have an organic component (associated with P). In the upper part of the map, Cl is distributed as discrete spots that correspond with similar spots of high Na concentrations. These spots continue with a similar distribution on the lower part of the mapped area. The most likely explanation for these spots is NaCl solution within micro–fluid inclusions. This clearly shows that in the cleaner speleothem calcite, Cl is incorporated solely within fluid inclusions, while in micritic calcite, Cl can be incorporated in fluid inclusions and associated with detrital material.

Incorporation of Cl into speleothem carbonate

The mechanism by which Cl is incorporated into carbonate speleothem fabrics seems to exert a major influence in determining its concentration and distribution, and thus its potential utility

as an archive of past Cl concentrations that could be used to reconstruct palaeo-infiltration and palaeo-meteoric ^{36}Cl/Cl ratios as a proxy for solar activity. We discount that Cl incorporates into the carbonate mineral lattice by substitution in the CO_3^{2-} sites due to the difference in size and electron density, rendering Cl^- incompatible in the calcite structure (Staudt et al., 1993; Temmam et al., 2000). Moreover, Figures 6–9 show ions that incorporate into the carbonate structure via ion substitution, such as Mg and S, tend to define the crystal faces, while Cl does not. Importantly, Figures 6 and 9 show evidence that we can interpret as Cl incorporation as fluid inclusions. This backs up the findings from water-leaching experiments that showed a water-soluble Cl component in all the samples (Fig. 4), at least in part derived from fluid inclusions visible in their thin sections (Figs. 2 and 3). However, the total Cl concentrations also contain a scarcely soluble Cl component (Fig. 4). In Figures 7–9, it is clear that Cl can be associated with particulate matter high in Al and Si, which may account for enrichment of Cl through detrital-associated Cl (i.e., the Cl is part of the composition of the particulate matter or is adsorbed onto the particulates) or authigenic clay-type mineral formation. This supports the finding that samples LC5 and CB41, having both high porosity (hosting Cl^- as fluid inclusions) and micrite laminae (incorporating Cl associated with particulate matter) (Fig. 2b and f), had the highest total Cl concentrations (Fig. 4). However, Figures 7 and 8 suggest that there could be alternative Cl incorporation mechanisms—other than fluid inclusions or particulate matter. Possible additional mechanisms of Cl incorporation include within defect sites compensating for charge imbalances, as Cl-bearing minerals involving elements not studied here, or associated with chlorinated organic compounds potentially including microbiological processes. The possibility could also arise whereby Cl is incorporated at defect sites, but the defects themselves may be formed due to the presence of particulates, organic compounds, or even bio-influenced crystallisation. These concepts require further research, for the case of Cl and additionally for other trace elements of palaeoclimatic significance.

Cl and ^{36}Cl as proxy records in speleothems

By using a variety of speleothems, we have shown that the presence of fluid inclusions and detrital particulates are important in controlling the incorporation and final concentration of Cl in speleothems. Hence, the Cl concentration stored within speleothems is not necessarily a reflection of the parent drip-water Cl^- concentrations. This means that any record of total Cl concentrations gained from a speleothem would not be a direct and quantifiable proxy of climatic or environmental variability, such as distance from the coast or evapotranspiration. Nonetheless, Cl concentrations could instead indicate changing fabrics, input of detritus and organics, or hiatuses. Still, these parameters may themselves be indicators of environmental conditions, for example, changes in cave ventilation, drip rate, infiltration-water calcite saturation state, surface vegetation changes, and runoff rate. Yet any links between these conditions and Cl concentrations would be, at this point, extremely tentative and warrant further investigation.

If the total Cl concentrations (by INAA) are considered, our leaching extraction method sometimes obtained low Cl yields, which is known to detrimentally affect isotope ratio measurements. However, due to the relatively small mass difference between the stable isotopes of Cl, the ^{37}Cl/^{35}Cl ratio shows little variability in the crustal environment; whereby the oceans are

characterised by a constant δ^{37}Cl ratio of 0‰, while evaporites are usually within 0.5‰ of the ocean values (Kaufmann et al., 1984; Sharp et al., 2007; Wang et al., 2019). The cosmogenic isotope ^{36}Cl lies between the masses of the two stable isotopes; therefore, the mass difference between ^{36}Cl and the stable isotopes is smaller than the difference between the two stable isotopes. Hence, negligible isotopic fractionation of ^{36}Cl/Cl is expected during incorporation into speleothems. Therefore, unlike total Cl concentrations in speleothems that do not reflect drip-water Cl concentrations, the ^{36}Cl/Cl ratio, because it is measured as a ratio, potentially reflects drip-water values and could possibly provide information regarding solar irradiance.

Moreover, for the analyses of ^{36}Cl/Cl ratios, only the water-soluble fraction is desired, because this reflects the meteoric signal that forms the proxy for solar activity. By contrast, the insoluble fraction comprises Cl that is strongly bound to detrital particulates and organic compounds, in which the Cl is of unknown age and may have been reworked and recycled and possibly transported long distances. Hence, this strongly bound Cl might not be representative of the ^{36}Cl/Cl ratio at the time of speleothem formation, and thus would not provide a proxy of solar irradiance. Paradoxically, the low-Cl speleothems in which a high fraction of the total Cl is likely to be hosted by fluid inclusions may provide the most reliable contemporaneous meteoric ^{36}Cl/Cl signals, although this presents challenges in terms of recovering sufficient Cl for AMS analysis.

The data presented in Table 3 have many possibilities for inaccuracies due to the low concentrations of Cl in the samples, the large amount of spike required, and the accuracy of dating. The final column of Table 3 roughly estimates the present-day ^{36}Cl/Cl ratio in rainwater at each site based on interpolation between a limited number of points across Europe at a single snapshot in time (Johnston and McDermott, 2008). However, despite all these uncertainties and the very limited data sets, in addition to the speleothems being deposited in the past when environmental conditions may have been different, the highest ^{36}Cl/Cl ratio in CB41 does mirror the high ^{36}Cl/Cl ratio in local rainfall in this central continental area, while the lowest ^{36}Cl/Cl ratio in TH1 corresponds with a low rainwater value at this site close to the coast. This provides a tentative proof of concept that the speleothem ^{36}Cl/Cl ratios reflect those of the meteoric water and can be measured successfully in speleothems.

A crucial issue is that, due to the unsystematic Cl incorporation, the total Cl concentration is not quantitatively linked to the atmospheric/drip-water Cl^{-} concentrations. Hence, this would negate the possibility of reconstructing quantitative ^{36}Cl fallout rates. Moreover, the fundamental problem is the low quantities of Cl incorporated into the speleothems and the inference above that the low-Cl samples may provide the most suitable material in terms of potentially recovering a contemporaneous meteoric water ^{36}Cl/Cl signal. Consequently, albeit theoretically feasible, the possibility of gaining a high-resolution time series of ^{36}Cl/Cl ratios from speleothems still requires advances in the current instrumental sensitivity for measuring ^{36}Cl/Cl ratios, significant advances in our understanding of Cl hosts in speleothems, and improvements in the techniques used for the extraction of meteoric Cl from speleothems.

CONCLUSIONS

We measured total Cl and water-soluble Cl^{-} concentrations and mapped Cl distribution at high resolution in speleothems from coastal and inland settings and from Holocene to Pleistocene age. In all samples, total Cl concentrations are relatively low, between 3 and 14 mg/kg, notably lower than marine, organic-rich, and fine-grained limestone. Our findings indicate that Cl incorporation into speleothem carbonates is very complex, and more than one mode of incorporation is responsible for the total Cl concentration within speleothems.

We propose that there are two different Cl fractions within speleothems: a water-soluble, loosely bound component and a water-insoluble, strongly bound constituent. The water-soluble fraction is made up of fluid inclusions and, potentially, also Cl that is loosely bound to the crystal lattice, possibly compensating for charge imbalances at defect sites. This fraction is extracted easily from speleothem carbonate by a simple water-leaching process. By contrast, the water-insoluble fraction is strongly bound to or within detrital particulates and water-insoluble organic compounds and is not extracted by water-based leaching but is apparent when measuring total Cl by INAA and visually obvious in trace element maps. Several of our samples had broadly similar concentrations of both water-soluble and total Cl, indicating that, in these samples, the majority of the Cl was loosely bound and water soluble. However, the speleothems with the highest total Cl concentrations were those that were strongly laminated and micritic, containing large amounts of detrital material, presumably including organic compounds.

Critically, the distribution of Cl at a micrometre-scale analysed by using synchrotron μ-XRF clearly showed the two different modes of Cl incorporation: in water-soluble fluid inclusions and bound to particulate matter. However, in some samples, the distribution of Cl could not be attributed to these incorporation mechanisms, thus indicating that Cl incorporation into speleothems is a complex system whereby other processes require consideration; for example, Cl incorporation at crystal defect sites, as noncarbonate Cl-bearing minerals, related to crystal growth mechanics (e.g., amorphous calcium carbonate precursors), or associated with chlorinated organic compounds potentially including microbiological processes. The main outcome of this study highlights a knowledge gap regarding the mechanisms by which trace elements are incorporated into carbonates of palaeoclimatic significance, requiring further research into the ways in which speleothem fabrics encode palaeoenvironmental signals.

Our findings include the first measurements of ^{36}Cl/Cl ratios on speleothems. The low concentrations of meteoric Cl present in our samples (which are likely representative of most speleothem samples) necessitated large sample sizes and a high proportion of spike, leading to significant spike corrections, resulting in large uncertainties. Our results are not encouraging for the aim of attaining a record of ^{36}Cl/Cl ratios to reconstruct past solar irradiance. Despite this, there is a rough connection between the ^{36}Cl/Cl ratios measured in the speleothems and the present-day ^{36}Cl/Cl ratios in rainwater. Therefore, with technological and methodological advances, along with good sample material, there is future potential to gain a ^{36}Cl/Cl ratio record from speleothems.

the PRIME Labs, Purdue, USA, for ^{36}Cl/Cl measurements and Becquerel labs Inc., Canada for INAA. Speleothem samples were generously donated by Ian Fairchild (Val-01), Galiba Sijarić (BHB04 and BMB06) and John Savage (TH1), and salt (NaCl) by Dave Lee. Matej Blatnik (IZRK ZRC-SAZU) kindly helped prepare the maps for Figure 1 and Tom Culligan (UCD) generously prepared thin sections for Figure 2.

REFERENCES

Baldini, L.M., Baldini, J.U.L., McDermott, F., Arias, P., Cueto, M., Fairchild, I.J., Hoffmann, D.L., *et al.*, 2019. North Iberian temperature and rainfall seasonality over the Younger Dryas and Holocene. *Quaternary Science Reviews* **226**, 105998.

Bard, E., Raisbeck, G.M., Yiou, F., Jouzel, J., 1997. Solar modulation of cosmogenic nuclide production over the last millennium: comparison between C-14 and Be-10 records. *Earth and Planetary Science Letters* **150**, 453–462.

Bastviken, D., Thomsen, F., Svensson, T., Karlsson, S., Sanden, P., Shaw, G., Matucha, M., Oberg, G., 2007. Chloride retention in forest soil by microbial uptake and by natural chlorination of organic matter. *Geochimica et Cosmochimica Acta* **71**, 3182–3192.

Beck, H.E., Zimmermann, N.E., McVicar, T.R., Vergopolan, N., Berg, A., Wood, E.F., 2018. Present and future Köppen-Geiger climate classification maps at 1-km resolution. *Scientific Data* **5**, 180214.

Beck, J.W., Richards, D.A., Edwards, R.L., Silverman, B.W., Smart, P.L., Donahue, D.J., Hererra-Osterheld, S., *et al.*, 2001. Extremely large variations of atmospheric C-14 concentration during the last glacial period. *Science* **292**, 2453–2458.

Borsato, A., Frisia, S., Fairchild, I.J., Somogyi, A., Susini, J., 2007. Trace element distribution in annual stalagmite laminae mapped by micrometer-resolution X-ray fluorescence: Implications for incorporation of environmentally significant species. *Geochimica et Cosmochimica Acta* **71**, 1494–1512.

Borsato, A., Johnston, V.E., Frisia, S., Miorandi, R., Corradini, F., 2016. Temperature and altitudinal influence on karst dripwater chemistry: implications for regional-scale palaeoclimate reconstruction from speleothems. *Geochimica et Cosmochimica Acta* **177**, 275–297.

Campbell, M., McDonough, L., Treble, P.C., Baker, A., Kosarac, N., Coleborn, K., Wynn P.M., Schmitt, A.K., 2023. A review of speleothems as archives for paleofire proxies, with Australian case studies. *Reviews of Geophysics* **61**, e2022RG000790.

Christl, M., Mangini, A., Holzkamper, S., Spötl, C., 2004. Evidence for a link between the flux of galactic cosmic rays and Earth's climate during the past 200,000 years. *Journal of Atmospheric and Solar-Terrestrial Physics* **66**, 313–322.

Coleman, J.C., 1965. *The Caves of Ireland.* Anvil Books, Tralee, Ireland.

Cornett, R.J., Andrews, H.R., Chant, L.A., Davies, W.G., Greiner, B.F., Imahori, Y., Koslowsky, V.T., Kotzer, T., Milton, J.C.D., Milton, G.M., 1997. Is Cl-36 from weapons' test fallout still cycling in the atmosphere? *Nuclear Instruments & Methods in Physics Research Section B: Beam Interactions with Materials and Atoms* **123**, 378–381.

Della Porta, G., 2015. Carbonate build-ups in lacustrine, hydrothermal and fluvial settings: comparing depositional geometry, fabric types and geochemical signature. *Geological Society of London Special Publication* **418**, 17–68.

Demény, A., Rinyu, L., Kern, Z., Hatvani, I.G., Czuppon, G., Surányi, G., Leél-Őssy, S., Shen, C-C., Koltai, G., 2021. Paleotemperature reconstructions using speleothem fluid inclusion analyses from Hungary. *Chemical Geology* **563**, 120051.

Duran, J., Lopez-Martinez, J., Dalai L., Bruschi, G., Caballero, E., Jimenz de Cisneros, C., Julia, R., 2000. Palaeoenvironmental reconstruction based on a detailed stable isotope analysis and dating of a Holocene speleothem from Valporquero Cave, northern Spain. *Geogaceta* **27**, 63–66.

Fairchild, I.J., Baker, A., Borsato, A., Frisia, S., Hinton, R.W., McDermott, F., Tooth, A.F., 2001. Annual to sub-annual resolution of multiple trace-element trends in speleothems. *Journal of the Geological Society of London* **158**, 831–841.

Fairchild, I.J., Treble, P.C., 2009. Trace elements in speleothems as recorders of environmental change. *Quaternary Science Reviews* **28**, 449–468.

Faraji, M., Frisia, S., Hua, Q., Borsato, A., Markowska, M., 2023. Accurate chronological construction for two young stalagmites from the tropical South Pacific. *Quaternary Geochronology* **74**, 101415.

Fernandez, A., Løland, M.H., Maccali, J., Krüger, Y., Vonhof, H.B., Sodemann, H., Meckler, A.N., 2023. Characterization and correction of evaporative artifacts in speleothem fluid inclusion isotope analyses as applied to a stalagmite from Borneo. *Geochemistry, Geophysics, Geosystems* **24**, e2023GC010857.

Frisia, S., 2015. Microstratigraphic logging of calcite fabrics in speleothems as tool for palaeoclimate studies. *International Journal of Speleology* **44**, 1–16.

Frisia, S., Borsato, A., Drysdale, R.N., Paul, B., Greig, A., Cotte, M., 2012. A re-evaluation of the palaeoclimatic significance of phosphorus variability in speleothems revealed by high-resolution synchrotron micro XRF mapping. *Climate of the Past* **8**, 2039–2051.

Frisia, S., Borsato, A., Fairchild, I.J., Susini, J., 2005. Variations in atmospheric sulphate recorded in stalagmites by synchrotron micro-XU and XANES analyses. *Earth and Planetary Science Letters* **235**, 729–740.

Frisia, S., Borsato, A., Hartland, A., Faraji, M., Demeny, A., Drysdale, R.N., Marjo, C.E., 2022. Crystallization pathways, fabrics and the capture of climate proxies in speleothems: Examples from the tropics. *Quaternary Science Reviews* **297**, 107833.

Frisia, S., Borsato, A., Hellstrom, J., 2018. High spatial resolution investigation of nucleation, growth and early diagenesis in speleothems as exemplar for sedimentary carbonates. *Earth-Science Reviews* **178**, 68–91.

Gallagher, S.J., Somerville, I.D., 1997. Late Dinantian (Lower Carboniferous) platform carbonate stratigraphy of the Buttevant area North Co. Cork, Ireland. *Geological Journal* **32**, 313–335.

Ivy-Ochs, S., Martin, S., Campedel, P., Hippe, K., Alfimov, V., Vockenhuber, C., Andreotti, E., *et al.*, 2017. Geomorphology and age of the Marocche di Dro rock avalanches (Trentino, Italy). *Quaternary Science Reviews* **169**, 188–205.

Jackson, A.S., 2009. Variable Sensitivity of European Holocene Speleothems to Climate Change: Case Studies from Selected Caves. Unpublished PhD thesis, University College Dublin, Dublin, Ireland.

Jackson, A.S., McDermott, F., Mangini, A., 2008. Late Holocene climate oscillations and solar fluctuations from speleothem STAL-AH-1, Sauerland, Germany: a numerical perspective. *Geophysical Research Letters* **35**, L06702.

Johnston, V.E., Borsato, A., Frisia, S., Spötl, C., Dublyansky, Y., Töchterle, P., Hellstrom, J.C., Bajo, P., Edwards, R.L., Cheng, H., 2018. Evidence of thermophilisation and elevation-dependent warming during the Last Interglacial in the Italian Alps. *Scientific Reports* **8**, 2680.

Johnston, V.E., Borsato, A., Spötl, C., Frisia, S., Miorandi, R., 2013. Stable isotopes in caves over altitudinal gradients: fractionation behaviour and inferences for speleothem sensitivity to climate change. *Climate of the Past* **9**, 99–118.

Johnston, V.E., Martín-Pérez, A., Skok, S., Mulec, J., 2021. Microbially-mediated carbonate dissolution and precipitation; towards a protocol for ex-situ, cave-analogue cultivation experiments. *International Journal of Speleology* **50**, 137–155.

Johnston, V.E., McDermott, F., 2008. The distribution of meteoric Cl-36 in precipitation across Europe in spring 2007. *Earth and Planetary Science Letters* **275**, 154–164.

Johnston, V.E., McDermott, F., 2009. Cosmogenic Cl-36 in karst waters: quantifying contributions from atmospheric and bedrock sources. *Geophysical Research Letters* **36**, L23705.

Kaufmann, R., Long, A., Bentley, H., Davis, S., 1984. Natural chlorine isotope variations. *Nature* **309**, 338–340.

Lal, D., Peters, B., 1967. Cosmic Ray Produced Radioactivity on the Earth. In: Sitte, K. (Ed.), *Kosmische Strahlung II/Cosmic Rays II. Handbuch der Physik/ Encyclopedia of Physics*. Vol. 9/46/2. Springer, Berlin. https://doi.org/10. 1007/978-3-642-46079-1_7.

Lechleitner, F.A., Fohlmeister, J., McIntyre, C., Baldini, L.M., Jamieson, R.A., Hercman, H., Gąsiorowski, M., *et al.*, 2016. A novel approach for

construction of radiocarbon-based chronologies for speleothems. *Quaternary Geochronology* **35**, 54–66.

Martín-García, R., Alonso-Zarza, A.M., Martín-Pérez, A., 2009. Loss of primary texture and geochemical signatures in speleothems due to diagenesis: evidences from Castañar Cave, Spain. *Sedimentary Geology* **221**, 141–149.

McDermott, F., 2004. Palaeo-climate reconstruction from stable isotope variations in speleothems: a review. *Quaternary Science Reviews* **23**, 901–918.

McDermott, F., Frisia S., Huang Y.M., Longinelli, A., Spiro, B., Heaton, T.H.E., Hawkesworth, C.J., et al., 1999. Holocene climate variability in Europe: Evidence from δ^{18}O, textural and extension-rate variations in three speleothems. *Quaternary Science Reviews* **18**, 1021–1038.

McDermott, F., Schwarcz, H., Rowe, P.J., 2005. Isotopes in speleothems. In: Leng, M.J. (Ed.), *Isotopes in Palaeoenvironmental Research*. Springer, Dordrecht, Netherlands, pp. 185–225.

Milanolo, S., Gabrovšek, F., 2009. Analysis of carbon dioxide variations in the atmosphere of Srednja Bijambarska Cave, Bosnia and Herzegovina. *Boundary-Layer Meteorology* **131**, 479–493.

Milanolo, S., Gabrovšek, F., 2015. Estimation of carbon dioxide flux degassing from percolating waters in a karst cave: case study from Bijambare cave, Bosnia and Herzegovina. *Geochemistry* **75**, 465–474.

Milton, G.M., Milton, J.C.D., Schiff, S., Cook, P., Kotzer, T.G., Cecil, L.D., 2003. Evidence for chlorine recycling—hydrosphere, biosphere, atmosphere —in a forested wet zone on the Canadian Shield. *Applied Geochemistry* **18**, 1027–1042.

Münsterer, C., Christl, M., Alfimov, V., Ivy-Ochs, S., Schröder-Ritzrau, A., Fohlmeister, J., Mangini, A., 2012. Cosmogenic ^{36}Cl in karst waters from Bunker Cave north western Germany—a tool to derive local evapotranspiration? *Geochimica et Cosmochimica Acta* **86**, 138–149.

Muscheler, R., Beer, R., Kubik, P.W., Synal, H.A., 2005. Geomagnetic field intensity during the last 60,000 years based on Be-10 and Cl-36 from the Summit ice cores and C-14. *Quaternary Science Reviews* **24**, 1849–1860.

Oldham A., 1981. *The Caves of Co. Cork*. Self-published, Crymych, Dyfed, Wales, p. 4.

Phillips, F.M, Leavy, B.D., Jannik, N.O., Elmore, D., Kubik, P.W., 1986. The accumulation of cosmogenic chlorine-36 in rocks: a method for surface exposure dating. *Science* **231**, 41–43.

Plummer, M.A., Phillips, F.M., Fabryka Martin, J., Turin, H.J., Wigand, P.E., Sharma, P., 1997. Chlorine-36 in fossil rat urine: an archive of cosmogenic nuclide deposition during the past 40,000 years. *Science* **277**, 538–541.

Polyak, V.J., Güven, N., 2004. Silicates in carbonate speleothems, Guadalupe Mountains, New Mexico, USA. In: Sasowsky, I.D., Mylroie, J. (Eds.), *Studies of Cave Sediments*. Springer, Boston, MA, pp. 303–311.

Scholz, D., Frisia, S., Borsato, A., Spötl, C., Fohlmeister, J., Mudelsee, M., Miorandi, R., Mangini, A., 2012. Holocene climate variability in northeastern Italy: potential influence of the NAO and solar activity recorded by speleothem data. *Climate of the Past* **8**, 1367–1383.

Sharp, Z.D., Barnes, J.D., Brearley, A.J., Chaussidon, T.P., Fischer, T.P., Kamenetsky, V.S., 2007. Chlorine isotope homogeneity of the mantle, crust and carbonaceous chondrites. *Nature* **446**, 1062–1065.

Shtober-Zisu, N., Schwarcz, H.P., Konyer, N., Chow, T., Noseworthy, M.D., 2012. Macroholes in stalagmites and the search for lost water. *Journal of Geophysical Research* **117**, F03020,

Sniderman, J.K., Woodhead, J.D., Hellstrom, J., Jordan, G.J., Drysdale, R.N., Tyler, J.J., Porch, N., 2016. Pliocene reversal of late Neogene aridification. *Proceedings of the National Academy of Sciences USA* **113**, 1999–2004.

Staudt, W.J., Oswald, E.J., Schoonen, M.A.A., 1993. Determination of sodium, chloride and sulfate in dolomites: a new technique to constrain the composition of dolomitizing fluids. *Chemical Geology* **107**, 97–109.

Stock, G.M., Granger, D.E., Sasowsky, I.D., Anderson, R.S., Finkel, R.C., 2005. Comparison of U–Th, paleomagnetism, and cosmogenic burial methods for dating caves: implications for landscape evolution studies. *Earth and Planetary Science Letters* **236**, 388–403.

Stone, J.O., Allan, G.L., Fifield, L.K., Cresswell, R.G., 1996. Cosmogenic chlorine-36 from calcium spallation. *Geochimica et Cosmochimica Acta* **60**, 679–692.

Temmam, M., Paquette, J., Vali, H., 2000. Mn and Zn incorporation into calcite as a function of chloride aqueous concentration. *Geochimica et Cosmochimica Acta* **64**, 2417–2430.

Tooth, A.F., Fairchild, I.J., 2003. Soil and karst aquifer hydrological controls on the geochemical evolution of speleothem-forming drip waters, Crag Cave, southwest Ireland. *Journal of Hydrology* **273**, 51–68.

Treble, P.C., Fairchild, I.J., Baker, A., Meredith, K.T., Andersen, M.S., Salmon, S.U., Bradley, C., et al., 2016. Roles of forest bioproductivity, transpiration and fire in a nine-year record of cave dripwater chemistry from southwest Australia. *Geochimica et Cosmochimica Acta* **184**, 132–150.

Turin, H.J., Plummer, M.A., Phillips, F.M., 2022. Tritium, Chlorine-36, and water isotopologue profiles from Lechuguilla Cave and Carlsbad Cavern, New Mexico, USA. *Applied Geochemistry* **138**, 105212.

Usoskin, I.G., Horiuchi, K., Solanki, S., Kovaltsov, G.A., Bard, E., 2009. On the common solar signal in different cosmogenic isotope data sets. *Journal of Geophysical Research* **114**, A03112.

Verheyden, S., Keppens, E., Fairchild, I.J., McDermott, F., Weis, D., 2000. Mg, Sr and Sr isotope geochemistry of a Belgian Holocene speleothem: implications for paleoclimate reconstructions. *Chemical Geology* **169**, 131–144.

Wang, Y., Hsu, W., Guan, Y., 2019. An extremely heavy chlorine reservoir in the Moon: insights from the apatite in lunar meteorites. *Scientific Reports* **9**, 5727.

Webb, J. A., James, J.M., 2006. Karst evolution of the Nullarbor Plain, Australia. In: Harmon, R.S., Wicks, C. (Eds.), *Perspectives on Karst Geomorphology, Hydrology, and Geochemistry—A Tribute Volume to Derek C. Ford and William B. White*. *Geological Society of America Special Paper* **404**, 65–78.

White, W.B., 2007. Cave sediments and paleoclimate. *Journal of Cave and Karst Studies* **69**, 76–93.

Woodhead, J.D., Sniderman, J.M., Hellstrom, J., Drysdale, R.N., Maas, R., White, N., White, S., Devine, P., 2019. The antiquity of Nullarbor speleothems and implications for karst palaeoclimate archives. *Scientific Reports* **9**, 603.